Publishing House
AKAPIT

COMPUTER METHODS IN MATERIALS SCIENCE

Informatyka w Technologii Materiałów

Vol. 17, 2017, No. 4

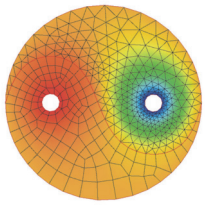

DEVELOPMENT OF THE MATERIAL DATABASE FOR THE VIRTROLL COMPUTER SYSTEM DEDICATED TO DESIGN OF AN OPTIMAL HOT STRIP ROLLING TECHNOLOGY

KRZYSZTOF BZOWSKI[5], JACEK KITOWSKI[1,5], ROMAN KUZIAK[2], PELLO URANGA[3], ISABEL GUTIERREZ[3], RONAN JACOLOT[4], ŁUKASZ RAUCH[5*], MACIEJ PIETRZYK[5]

[1]ACC Cyfronet AGH, AGH University of Science and Technology, Krakow, Poland.
[2]Institute for Ferrous Metallurgy, ul. K. Miarki 12, 44-100 Gliwice, Poland.
[3]CEIT Paseo de Manuel Lardizabal 15, 20018 Donostia-San Sebastián, Spain
[4]ArcelorMittal Maizières Research SA, Voie Romaine, 57280 Maizières-lès-Metz, France
[5]AGH University of Science and Technology, al. Mickiewicza 30, 30-059 Kraków, Poland
**Corresponding author: lrauch@agh.edu.pl*

Abstract

The paper describes the material database, which was developed and included in the VirtRoll computer system dedicated to the design of optimal hot strip rolling technologies. The structure and functionalities of the database are described in the first part of the paper. The integration between the database and the system through the Scalarm platform is described next. Following chapters are dedicated to generation of material data, which are included in the database. These data are coefficients in material models, which include flow stress models, microstructure evolution models, phase transformation models and mechanical properties models. Several models of various complexity and various predictive capabilities were chosen for each mentioned phenomenon. All are mean field models to allow fast simulation of the whole manufacturing chain. Modern multiphase steels grades were selected as the case studies. Experimental tests performed to generate the data composed plastometric tests, stress relaxation tests and dilatometric tests. Inverse analysis was applied to determine the coefficients in the model. Discussion of results focused on validation and on new aspects of models recapitulates the paper.

Key words: Hot strip rolling, Material data base, Material models, Identification

1. INTRODUCTION

Studying rolling-related processes, by building a virtual hot rolling mill, can be described as a multi-step workflow involving:

- design of a virtual hot rolling mill,
- simulation of the rolling process with the parameter study approach,
- output data exploration with sensitivity analysis methods to discover relationships between the hot rolling mill parameters and the obtained thermo-mechanical properties in final product.

Each of these steps has different requirements regarding easiness of use, computing power and progress monitoring. Designing and developing of a system supporting this multi-step workflow was the main objective of the whole project.

Problem of the computer aided design of the hot strip rolling technology has been in the field of interest of researchers for more than half of the century. The first fundamental works in this field were focused on development of Thermo-Mechanically Controlled Process (TMCP), which required the development of both metallurgical (Sah & Sellars, 1979; Nanba et al., 1992; Novillo et al., 2005) and

ISSN 1641-8581

numerical models (Beynon & Sellars, 1992; Hodgson & Gibbs, 1992; Zurob et al., 2005). Following development of the computing power microstructure evolution models were implemented in the finite element (FE) codes and fully coupled thermal-mechanical-metallurgical simulations became possible (Pietrzyk, 1990). In late 1990-ties and at the beginning of this century several through process models describing the whole manufacturing process were developed (Donnay et al., 1996; Pietrzyk, 2002; Uranga, 2004).

The first models developed half of the century ago had serious limitations when applied under conditions different from those for which they were developed (short interpass times, privilege recovery over recrystallization). Current models became more reliable and accurate. The steel industry nowadays needs developing AHSS (Advanced High Strength Steel) grades in a cost-effective way and get them to market as fast as they can while manufacturing them within the constraints of their mill configuration. This needs progress in terms of modelling to be performed, allowing for example effective modelling of new tendencies as eg. the low coiling temperatures required for hot rolled Dual Phase steel. The mentioned models limitations justified creation of a computer system dedicated to flexible design and modelling of hot rolling technology. Some such systems based on hot rolling metallurgical models have been developed and used for defining thermo-mechanical cycles or monitoring the mechanical properties. Worldwide experiences are reported in the literature (Löffler et al., 2001; Lotter et al., 2004; Andorfer et al., 1998). Software packages such as TK-StripCam by ThyssenKrupp Stahl (Lotter et al., 2004), MetModel by Corus (Trowsdale et al., 2001), MicroStructureMonitor by Siemens (Löffler et al., 2001), VAI-Q strip (Andorfer et al., 1998) by Voestalpine and Industrieanlagenbau (VAI) and HSMM (Ibrahim & Shulkosky, 2007) by the INTEG process group are available. The system Slimmer commonly used in the industry is described in (Beynon & Sellars, 1992; Donnay et al., 1996). Authors, model was applied in (Kuziak & Pietrzyk, 2011) to simulation of hot DP steel strip rolling. All these packages are based on direct approach. They are not integrated with knowledge bases and inverse solutions based on the optimization techniques.

Review of the literature shows that currently available systems predict accurately the deformation behaviour for typical rolling routes. New tendencies in development of rolling strategies, such as high austenite deformations near two-phase region or bainite evolution in coils, are still a challenge. Thus, over the last few years, more attention has been paid to the models that can predict the microstructural evolution during hot rolling, subsequent cooling and coiling, followed by the prediction of mechanical properties in the room temperature. The goal is usually to predict the microstructure of the materials and to optimize the process conditions to obtain the best combination of strength, ductility and weldability in the as-rolled product. The computer system VirtRoll developed by the Authors (Rauch et al., 2016) was designed to face all mentioned above challenges.

The VirtRoll system combines models, data and knowledge bases and inverse approach to design of optimal processes. It allows design of rolling line composed of basic equipment like furnace, descalers, rolling stands, laminar cooling, coilers, etc. Dependently on selected materials specific numerical models can be loaded by the system. The main loading procedure is based on the workflow idea and supported by software framework for workflow design, creation and performance. This approach was integrated with the steel modelling workbench, which is an open software environment, where various models can be linked and run to allow the modular development of integrated models of various stages of the manufacturing. The integration was based on the common data flow model. An overview of the system along with main steps of the workflow is depicted in figure 1. Numerical simulations of different hot rolling aspects are an essential part of studying rolling-related processes.

As it has been mentioned, combination of models with the data and knowledge bases and with the inverse approach to design of optimal processes is the main advantage of the VirtRoll system, which distinguishes this system from the existing ones. Development of the database and application of the inverse analysis to identification of various material models was the main objective of this paper.

2. DATABASE

The work was started with the analysis of the software architecture, which was used as a fundamental element of the VirtRoll system dedicated to flexible material modelling, large scale computations, sensitivity analysis and optimization. All the analysed aspects of the architecture influence final

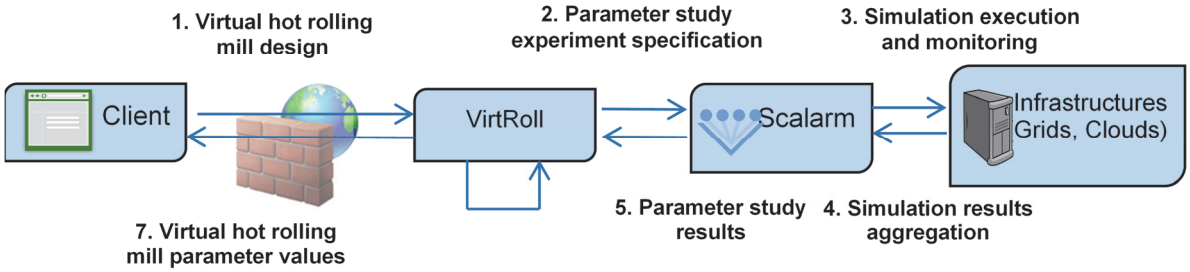

Fig. 1. *An overview of a system supporting studying workflow of hot strip rolling processes.*

design and implementation of the database including: authorization and authentication, process design and parameters selection, materials management, computing jobs performance, monitoring and many others. This also includes storing of common data used by all subsystems, which are crucial for using modern e-infrastructures.

2.1. Methodology

The technology involved in the paper concerns three main elements: the VirtRoll system development, the integration between the system and the Scalarm platform (Król et al., 2014) as well as numerical simulations of rolling-related processes.

VirtRoll is composed of two parts (Rauch et al., 2016) i.e. a web-based module allowing design of rolling mill and computing module dedicated to numerical simulations of designed manufacturing cycle. Information about materials and devices available for hot rolling mill designers is stored in the database, being the aim of this paper. The idea was to design the database to be as flexible as possible, therefore, MongoDB was used in the first implementation. The selection of database management system MongoDB was justified mainly by its capability of object oriented design and implementation convergent with model layer in application. This choice was dictated by the compatibility of the database with the server side of the system and the maintenance of flexible data modelling of the process, i.e. support for new materials and devices, characterized by different parameters. The schematic illustration of the structure of the database is shown in figure 2. The component dedicated to *Designs* contains the following collections of:

- designs, which remain in relation many-to-one with the collection of projects, containing various information on different design within the same project,
- elements of the project including devices, optimization and sensitivity analysis, which are related to the specific design,
- information on calculations, which are connected with the experiments performed in Scalarm system – these collections are related to single simulations, optimization and sensitivity analysis.

The component holding collections for User data includes credentials for both systems i.e. VirtRoll and Scalarm. It is crucial to hold this information from the point of view of the numerical simulations, which in form of experiments are submitted to the HPC infrastructures. Each of such infrastructures requires further authentication and authorization what is supported by the designed database. The rest of the database stores information on materials and models including chemical composition of the material, as well as all the parameters of material models. Due to such solution it is possible to access these parameters through the Graphical User Interface (GUI) to make them available for computational module.

2.2. Materials

In the present project the material data for four groups of steels were introduced into the database. Few heats were prepared in each group, distinguished by the additions of Nb, Ti and Mo:

- HSLA steels with 0.035%Nb (S401, S408), 0.035%Nb + 0.2%Mo (S403) and 0.035%Nb + 0.09%Ti + 0.2%Mo (S404).
- Bainitic steels with 0.12%Ti + 0.2%Mo (S405), 0.18%Ti + 0.2%Mo (S406) and 0.03%Nb + 0.18%Ti + 0.2%Mo (S407).
- Dual Phase (DP) steels with 0.034%Nb + 0.001%Ti + 0.02%Mo (S447), 0.036%Nb (S448) and 0.037%Nb + 0.002%Ti + 0.03%Mo (S448).
- Advanced High Strength Steels with 0.035%Nb (AHSS-9), 0.035%Nb + 0.2%Mo (AHSS-10), 0.13%Ti (AHSS-11) and 0.13%Ti + 0.2%Mo (AHSS-12).

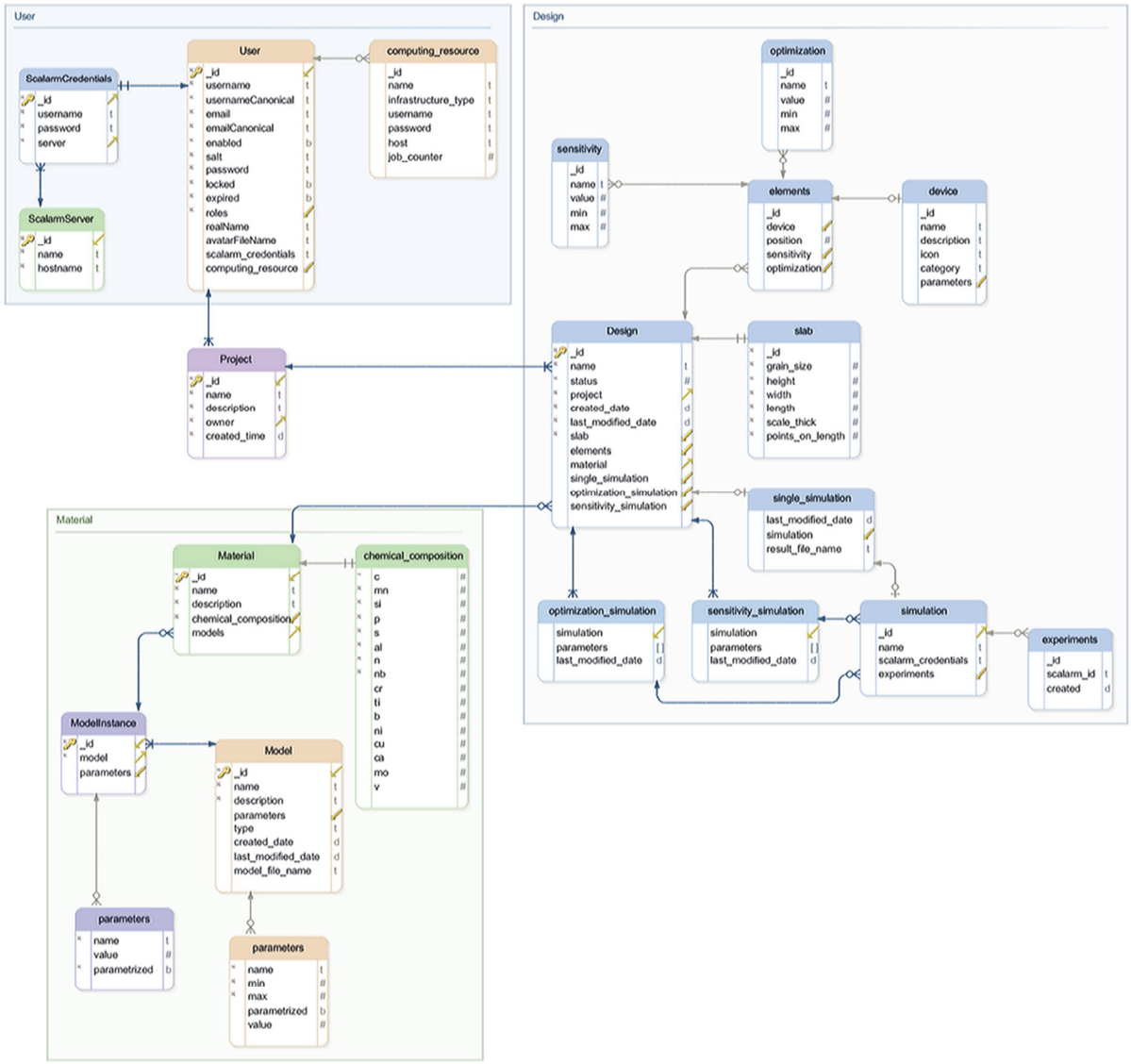

Fig. 2. *Structure of the VirtRoll database*

3. MODELS

Rolling models implemented into the VirtRoll system are presented in (Rauch et al., 2016) and they are not discussed here. The objective of this part is presentation of material models, which were implemented into the database. Procedure of the identification of all models on the basis of experiments is described, as well. The models were divided into four groups:

- Flow stress models
- Microstructure evolution models
- Phase transformation models
- Models describing mechanical properties of products.

Since the VirtRoll system is dedicated to the industrial applications, selection of the models was made using the computing costs as the main criterion. Authors have developed models of various complexity and various predictive capabilities ranging from closed form equations to advanced multiscale models base on discrete methods. Problems of the balance between the predictive capabilities and computing costs of various models is discussed in (Pietrzyk et al., 2015). In the following Sections simple models with reasonably good predictive capabilities are presented.

3.1. Flow stress

Five models of various complexity and various predictive capabilities were implemented in the VirtRoll system. The simplest is a typical equation accounting for the influence of temperature, strain and strain rate:

$$\sigma_p = A\varepsilon^n \dot{\varepsilon}^m \exp\left(\frac{Q_{def}}{RT}\right) \qquad (1)$$

where: σ_p — flow stress, $\dot{\varepsilon}$ – strain rate, ε – strain, Q_{def} – activation energy of deformation, T – temperature in K, R – universal gas constant.

Equation (1) does not account for softening due to dynamic recrystallization. Thus, Hensel-Spittel equation (Hensel & Spittel, 1979) was used to overcome this disadvantage:

$$\sigma_p = A\varepsilon^n \exp(q\varepsilon)\dot{\varepsilon}^m \exp(-\beta T_C) \qquad (2)$$

where: T_C – temperature in °C.

Three more advanced models with a capability to describe properly the peak stress as well as stress saturation for larger strains were additionally included into the database:

– Model proposed by Gavrus et al. (1996):

$$\sigma_p = \sqrt{3}\left[WK\varepsilon^n \exp\left(\frac{-Q}{RT}\right) + (1-W)K_{sat}\exp\left(\frac{Q_{sat}}{RT}\right)\right]\left(\sqrt{3}\dot{\varepsilon}\right)^m \qquad (3)$$

where: $W = \exp(-q\varepsilon)$

– Sellars-Teggart (S-T) model (Sellars & McTegart, 1966) described also in (Davenport et al., 1999; Kowalski et al., 2000):

$$\sigma_p = \sigma_0 + \left(\sigma_{ss(e)} - \sigma_0\right)\left[1 - \exp\left(-\frac{\varepsilon}{\varepsilon_r}\right)\right]^{\frac{1}{2}} - C \qquad (4)$$

where:

$$C = \begin{cases} 0 & \varepsilon \le \varepsilon_c \\ \left(\sigma_{ss(e)} - \sigma_{ss}\right)\left[1 - \exp\left(-\left[\frac{\varepsilon - \varepsilon_c}{\varepsilon_{xr} - \varepsilon_c}\right]^2\right)\right] & \varepsilon > \varepsilon_c \end{cases}$$

$$\sigma_0 = \frac{1}{\alpha_0}\sinh^{-1}\left(\frac{Z}{A_0}\right)^{\frac{1}{n_0}} \quad \sigma_{ss} = \frac{1}{\alpha_{ss}}\sinh^{-1}\left(\frac{Z}{A_{ss}}\right)^{\frac{1}{n_{ss}}}$$

$$\sigma_{sse} = \frac{1}{\alpha_{sse}}\sinh^{-1}\left(\frac{Z}{A_{sse}}\right)^{\frac{1}{n_{sse}}}$$

$$\varepsilon_r = \frac{1}{3.23}\left[q_1 + q_2\left(\sigma_{ss(e)}\right)^2\right]$$

$$\varepsilon_{xr} - \varepsilon_c = \frac{\varepsilon_{xs} - \varepsilon_c}{1.98}$$

$$\varepsilon_c = C_c\left(\frac{Z}{\sigma_{ss(e)}^2}\right)^{N_c}$$

$$\varepsilon_{xs} - \varepsilon_c = C_x\left(\frac{Z}{\sigma_{ss(e)}^2}\right)^{Nx}$$

where: ε_c – critical strain for dynamic recrystallization, Z – Zener-Hollomon parameter calculated as:

$$Z = \dot{\varepsilon}\exp\left(\frac{Q_{def}}{RT}\right) \qquad (5)$$

with Q_{def} – activation energy of deformation.

– Model developed in CEIT, which is an adaptation of the S-T model extended to account for the austenite grain size and for the effect of microalloying elements:

$$\sigma_p = \sigma_0 + \sigma_{ss}\left[1 - \exp(-\beta\varepsilon)\right]^{0.5} - C\sigma_{ss} \qquad (6)$$

where:

$$\beta = a_\beta - b_\beta \lg(Z)$$

$$C = \begin{cases} 0 & \varepsilon \le \varepsilon_c \\ 0.15X_{DRX} & \varepsilon > \varepsilon_c \end{cases}$$

$$\varepsilon_c = C_c\left[1 + 20\left([\mathrm{Nb}] + 0.02[\mathrm{Ti}] + \Delta\right)\right]D_0^{q_1}Z^{N_1}$$

$$\varepsilon_s = \varepsilon_c + C_x\left[1 + 20\left([\mathrm{Nb}] + 0.02[\mathrm{Ti}] + \Delta\right)\right]D_0^{q_2}Z^{N_2}$$

X_{DRX} above is the dynamically recrystallized volume fraction defined in Section 3.2. Coefficient Δ is equal to 0.035 for Nb and Ti+Mo steels S403 and S404 and is equal zero for the remaining steels. Symbols ε_c, σ_{ss} are defined under equation (4).

3.2. Microstructure evolution

Conventional equations describing microstructure evolution during hot rolling as well as ferrite grain size were used as the default models in the VirtRoll database. The review of these models as well as coefficients for various conventional steels can be found in (Lenard et al., 1999).

Certain minimum threshold of strain is needed to initiate the static recrystallization. This threshold is usually assumed $\varepsilon_{cr\text{-}SRX}$ = 0.03. General JMAK (Johnson-Mehl-Avrami-Kolmogorov) equation for kinetics of static recrystallization has a form:

$$X = 1 - \exp\left[-a\left(\frac{t}{t_b}\right)^n\right] \qquad (7)$$

where: n – Avrami exponent, a – coefficient.

Value of the coefficient a depends on the time t_b, which is a basic time in equation (7). It can be shown that:

$$a = \ln(1-b) \tag{8}$$

In equation (8) b is a recrystallized volume fraction for the basic time in equation (7). If, as suggested by Sellars (1979), time for 50% recrystallization $t_{0.50}$ is used as a basic time, then $b = 0.5$ and $a = 0.693$ and equation (7) applied to describe kinetics of the static recrystallization becomes:

$$X_{SRX} = 1 - \exp\left[-0.693\left(\frac{t}{t_{0.50}}\right)^n\right] \tag{9}$$

Time for 50% recrystallization in equation (9) is a function of process parameters:

$$t_{0.50} = A\varepsilon_i^{-a_1}\dot{\varepsilon}_i^{-a_2} D_0^{a_3} \exp\left(\frac{Q_{SRX}}{RT}\right) \tag{10}$$

where: ε_i – effective strain, $\dot{\varepsilon}_i$ – effective strain rate, D_0 – grain size prior to deformation, T – temperature in K.

For microalloyed steels S401, S402 and S403 time for 50% recrystallization in equation (9) is given by the following equation:

$$t_{0.50} = A\varepsilon_i^{-a_1 D_0^{-0.15}}\dot{\varepsilon}_i^{-a_2} D_0^{a_3} \exp\left(\frac{Q_{SRX}}{RT}\right)$$
$$\exp\left[\left(\frac{275000}{T} - 185\right)\left([\mathrm{Nb}]_{eff} + 0.374\right)[\mathrm{Ti}]\right] \tag{11}$$

where: ε_i – effective strain, $\dot{\varepsilon}_i$ – effective strain rate, D_0 – grain size prior to deformation, T – temperature in K.

The grain size after static recrystallization is calculated from the equation:

$$D_{SRX} = B\varepsilon^{-b_1}\dot{\varepsilon}^{-b_2} D_0^{b_3} \exp\left(\frac{-Q_{DSRX}}{RT}\right) \tag{12}$$

The total time of recrystallization is calculated assuming that recrystallization is completed when recrystallized volume fraction reaches 0.95. Thus, when $t_{0.50}$ is used as basic time, the total time of recrystallization is:

$$t_{SRX} = t_{0.95} = \left[\frac{\ln(0.05)}{\ln(0.5)}\right]^{\frac{1}{n}} t_{0.50} = 4.3219^{\frac{1}{n}} t_{0.50} \tag{13}$$

When the total time for recrystallization is shorter than the interpass time t_i ($t_{SRX} < t_i$), the grain growth is simulated during the remaining time ($t = t_i - t_{SRX}$). The following equation is used:

$$D_t^s = D_{t0}^s + K\,t \exp\left(-\frac{Q_{GROWTH}}{RT}\right) \tag{14}$$

where: D_{t0} – grain size at the beginning of growth, D_t – grain size after the time t.

When recrystallization is not completed before the next pass ($t_{SRX} > t_i$), partial recrystallization is simulated. The grain size at the entry to the next pass is calculated as a weighted average of the initial grain size D_0 and recrystallized grain size D_{SRX}, according to the formula:

$$D_1 = D_{SRX} X_{SRX} + D_0\left(1 - X_{SRX}\right) \tag{15}$$

When partial recrystallization takes place, some retained strain remains in the material. This strain is calculated as:

$$\varepsilon_{i+1} = W\varepsilon_i\left(1 - X_{SRX}\right) \tag{16}$$

where: ε_{i+1} – retained strain at the exit to the next pass, ε_i – effective strain in the previous pass, W – coefficient, which is usually taken as 1, but some of researchers use this coefficient to account for the influence of the recovery (Hodgson & Gibbs, 1992) and then $W < 1$.

Microstructure evolution model for static recrystallization contains several coefficients, which are identified on the basis of experimental tests. As it has been mentioned, stress relaxation were used for that purpose in the present work. The coefficients in kinetics and grain size equation obtained for selected steels are given in Section 5.2.

Dynamic recrystallization is the phenomenon, which involves controversies. The general understanding of the distinction between static and dynamic recrystallization is that the latter occurs during deformation and the former after the deformation, but the mechanism is in general the same. Interesting discussion of controversies connected with the dynamic recrystallization can be found in (McQueen, 1993) and thorough analysis of the phenomena occurring during dynamic recrystallization as well as modelling aspects are presented in (Zahiri & Hodgson, 2004). There is a general opinion that

when strain in a pass exceeds certain critical value the dynamic recrystallization begins during the deformation. This critical strain is defined under equation (4). Accounting for the austenite grain size leads to the following equation:

$$\varepsilon_{cr\_DRX} = p_1 D_0^{p_2} Z^{p_3} \tag{17}$$

Recrystallized volume fraction in dynamic recrystallization is a function of strain and is calculated as:

$$X_{DRX} = 1 - \exp\left[-p_7 \left(\frac{\varepsilon - \varepsilon_{cr\_DRX}}{\varepsilon_s - \varepsilon_{cr\_DRX}} \right)^{p_8} \right] \tag{18}$$

where: ε_s – saturation strain given by:

$$\varepsilon_s = p_4 D_0^{p_5} Z^{p_6} \tag{19}$$

In the present project for the HSLA steels (S401, S403 and S404) the following relation of the saturation strain on micro alloying elements was proposed:

$$\varepsilon_s = 5\times10^{-4} \frac{1 + 20\left([Nb] + 0.02[Ti] + 0.035\Delta\right)}{1.78} D_0^{p_5} Z^{p_6} + \varepsilon_c \tag{20}$$

Dynamically recrystallized volume fraction at the end of deformation is determined next. Strain in a pass ε_i is substituted for ε in equation (18) and the final volume fraction $X_{DRX}(\varepsilon_i)$ is calculated. It is again assumed that recrystallization is completed if the recrystallized volume fraction exceeds 0.95. If $X_{DRX}(\varepsilon_i) < 0.95$, the static recrystallization takes place in the remaining volume fraction $(1 - X_{DRX}(\varepsilon_i))$.

Dynamically recrystallized material is subjected to metadynamic recrystallization with the kinetics calculated from the equation:

$$X_{MDRX} = 1 - \exp\left[-0.693 \left(\frac{t}{t_{0.50}^{MDRX}} \right)^{q_1} \right] \tag{21}$$

where the time for 50% of the metadynamic recrystallization for the HSLA steels is (Elwazri, 200$):

$$t_{0.5}^{MDRX} = q_2 \dot{\varepsilon}^{-q_3} \exp\left(\frac{Q_{MDRX}}{RT} \right) \tag{22}$$

And for the remaining steels in this work:

$$t_{0.5}^{MDRX} = q_2 Z^{-q_3} \exp\left(\frac{Q_{MDRX}}{RT} \right) \tag{23}$$

The grain size after the dynamic recrystallization does not depend on the strain and is the function of the Zener-Hollomon parameter Z only:

$$D_{DRX} = p_9 Z^{-p_{10}} \tag{24}$$

Similar equation with different coefficients was proposed for the metadynamic recrystallization:

$$D_{MDRX} = q_4 Z^{-q_5} \tag{25}$$

Coefficients in equations describing the dynamic recrystallization and the metadynamic recrystallization are given in Section 5.2. When metadynamic recrystallization occurs, the grain size after completing the recrystallization is calculated as a weighted average of the grain size after dynamic recrystallization D_{DRX} and after the metadynamic recrystallization D_{MDRX}, according to the formula:

$$D_1 = D_{DRX} X_{DRX} + D_{MDRX} \left(1 - X_{DRX}\right) \tag{26}$$

When the dynamic or metadynamic recrystallization is completed, the grain growth is simulated in the remaining time. The grain growth equation (14) is used.

Models of transformations during cooling are described in the next Section. Ferrite grain size, which is used to determine mechanical properties of product, is calculated from the simplified model. Equation proposed by Hodgson and Gibbs (1992) accounting for the cooling rate and the austenite grain size was used as basic ferrite grain size model:

$$D_\alpha = \left(f_0 + f_1 C_{eq}\right) + \left(f_2 + f_3 C_{eq}\right) C_r^{0.5} + f_4 \left[1 - \exp\left(-f_5 D_\gamma\right)\right] \tag{27}$$

where: C_{eq} – carbon equivalent calculated as [C] + [Mn]/6, C_r – cooling rate calculated as an average during ferrite transformation, D_γ – austenite grain size at the beginning of the phase transformation.

Accounting for the austenite deformation at the beginning of the phase transformations is crucial for the accuracy of simulations. The following approach is commonly used:

$$D_{\alpha r} = \left(1 - 0.4\sqrt{\varepsilon_r}\right) D_\varepsilon \tag{28}$$

where: $D_{\alpha r}$ – ferrite grain size accounting for the retained strain in the austenite, D_α - ferrite grain size calculated from equation (27), ε_r - retained strain in the austenite at the beginning of the phase transformation.

3.3. Phase transformations

Two phase transformation models were implemented into the database. The first is an upgrade of the JMAK equation and the second is based on the control theory and describes the kinetic of phase transformations using the second order differential equation. Both models were described in earlier publications. The former in (Pietrzyk & Kuziak, 2012) and the latter, which will be referred to as CONT model, in (Milenin et al., 2015). Therefore, very brief information about the models is given below. JMAK equation (7) adapted to the phase transformation has the form:

$$X = 1 - \exp\left(-kt^n\right) \tag{29}$$

where: n – Avrami exponent, k – coefficient.

The following upgrades of this equation were introduced in the present work:

- Avrami coefficient n is assumed constant for each transformation (the first row in table 1).
- Coefficient k for ferrite, pearlite and bainite transformations was introduced as a function of temperature, as shown in (Donnay et al., 1996; Pietrzyk & Kuziak, 2012). Modified Gauss function was used for the ferrite transformation (Donnay et al., 1996). Nose of this function is located at the temperature of maximum rate of the transformation. Exponential functions were used for pearlite and bainite transformations (Pietrzyk & Kuziak, 2012), see the second row in table 1.
- Using Gauss function for k_f does not require the incubation time. It is assumed that ferrite transformation begins when 5% of ferrite is predicted by equation (29).
- Calculations of carbon concentration in the austenite during both ferrite and bainite transformations were added. In consequence prediction of the occurrence of the retained austenite became possible. Equations describing the incubation time for pearlite and bainite are given in the third row in table 1.
- The T_0 temperature concept was added (Bhadeshia, 1988). The T_0 curve is the locus of points on the temperature vs. carbon concentration plot where austenite and ferrite of the same chemical composition have identical free energies. This concentration is a boundary condition for calculation of the carbon distribution in the austenite using diffusion model.

Remaining equations in the model describe start temperatures for bainite (B_s) and martensite (M_s), volume fraction of martensite (V_m) and equilibrium carbon concentrations at the austenite-ferrite ($c_{\gamma\alpha}$) and the austenite-cementite ($c_{\gamma\beta}$) boundaries:

$$B_s = a_{20} - 425[\mathrm{C}] - 42.5[\mathrm{Mn}] - 31.5[\mathrm{Ni}] \tag{30}$$

$$M_s = a_{25} - a_{26}c_\gamma \tag{31}$$

$$V_m = \left(1 - V_f - V_p - V_b\right)\left\{1 - \exp\left[-0.011\left(M_s - T\right)\right]\right\} \tag{32}$$

where: V_f, V_p, V_b, V_m, – volume fractions of ferrite, pearlite, bainite and martensite, respectively, calculated with respect to the whole volume of the material.

Equation (29) combined with the Scheil additivity rule allows to calculate changes of volume fraction of the new phase during transient state between

Table 1. *Main equations in the phase transformation model*

Ferrite	Pearlite	Bainite
$n = a_4$	$n = a_4$	$n = a_4$
$k_f = \frac{a_5}{D_\gamma}\exp\left[-\left(\frac{\left\lvert T - A_{e3} - \frac{400}{D_\gamma} + a_6\right\rvert}{a_7}\right)^{a_8}\right]$	$k_p = a_{15}$	$k_b = a_{23}\exp\left[\left(\frac{T - a_{21}}{a_{22}}\right)^2\right]$
-	$\tau_P = \frac{a_9}{\left(\mathrm{A}_{e1} - T\right)^{a_{11}}}\exp\left(\frac{a_{10}}{RT}\right)$	$\tau_b = \frac{a_{17}}{\left(B_s - T\right)^{a_{19}}}\exp\left(\frac{a_{18}}{RT}\right)$

the two equilibrium states. Equilibrium carbon concentrations at the austenite-ferrite ($c_{\gamma\alpha}$) and austenite-cementite ($c_{\gamma\beta}$) interfaces are calculated from the following equations:

$$\begin{aligned} c_{\gamma\alpha} &= c_{\gamma\alpha 0} + c_{\gamma\alpha 1} T \\ c_{\gamma\beta} &= c_{\gamma\beta 0} + c_{\gamma\beta 1} T \end{aligned} \tag{33}$$

Details of the numerical solution of this phase transformation model are given in (Pietrzyk & Kuziak, 2012). Briefly, modelling starts with equation (29) when the temperature drops below A_{e3}. The ferrite volume fraction X_f is calculated with respect to the maximum volume fraction of this phase in steel V_{fmax}. Thus, the volume fraction of ferrite with respect to the whole volume of the material is $V_f = X_f V_{fmax}$ for the fixed temperature T. The value of X_f calculated from equation (29) for the varying temperature has to be corrected due to a change of the equilibrium ferrite volume fraction V_{fmax}, which is the function of temperature:

$$V_{f\max} = \frac{c_{\gamma\alpha} - c_0}{c_{\gamma\alpha} - c_\alpha} \tag{34}$$

where: c_0 – carbon concentration in the steel, c_α – carbon concentration in the ferrite.

The correction of X_f is made as follows:

$$X_f\left(T_{i+1}\right) = X_f\left(T_i\right) \frac{V_{f\max}\left(T_i\right)}{V_{f\max}\left(T_{i+1}\right)} \tag{35}$$

Average carbon content in the austenite (c_γ) increases with increasing volume fraction of ferrite:

$$c_\gamma = \frac{\left(c_0 - X_f c_\alpha\right)}{1 - X_f} \tag{36}$$

Simulation continues until the transformed volume fraction achieves 1. However, when carbon content in the austenite exceeds the limiting value ($c_{\gamma\beta}$), the pearlite transformation begins in the remaining austenite. For faster cooling bainitic transformation occurs.

Accounting for changes of carbon concentration in the austenite during bainitic transformation is another upgrade of the JMAK model. The current average carbon content in the austenite during bainitic transformation is described by the following equation:

$$c_\gamma = \frac{\left[c_0 - \left(V_f + \dfrac{V_b}{1-p}\right) c_\alpha\right]}{1 - V_f - \dfrac{V_b}{1-p}} \tag{37}$$

In equation (37) p represents probability that a new platelet of the bainitic ferrite forms in a close neighbourhood of the existing one and its diffusion field is constrained by this neighbour. This probability is well explained by Katsamas and Haidemenopoulos (2008) and the details of the numerical solution of the present model are given in (Pietrzyk et al., 2016).

The idea of the second phase transformation model is based on the Leblond equation (Leblond & Devaux, 1984). The main assumption of Leblond was that the rate of the transformation is proportional to the distance from the equilibrium. The first order differential equation with respect to time was obtained. This equation could not reproduce delay of the response due to nucleation and it required introduction of the incubation time. To avoid this problem the second order differential equation was proposed in (Milenin et al., 2015). It was based on the description of the second order inertia term in the control theory, therefore, this model is referred to as the CONT model. The volume fraction of the new phase X is calculated by the solution of the following equation:

$$B_1^2 \frac{d^2 X}{dt^2} + B_2 \frac{dX}{dt} + X = \mathrm{f}\left(T\right) \tag{38}$$

where: B_1, B_2 – time constants.

In equation (38) X is the volume fraction of the phase with respect to the maximum volume fraction of this phase in a considered temperature. For ferrite transformation we have:

$$\mathrm{f}\left(T\right) = \frac{V_{f\max}\left(T\right)}{V_{f\_eut}} \tag{39}$$

where: $V_{fmax}(T)$ – maximum volume fraction of ferrite in the temperature T, V_{f_eut} – volume fraction of ferrite in steel, calculated from equation (34) at the eutectic point.

In order to describe phenomena of nucleation and growth, the two time constants were introduced in the model and were based on the mathematical description of the second order inertia term. Time constant B_1 is responsible for the delay of the response in the initial stage of transformation, therefore, it was correlated with the nucleation rate. Since

this rate directly depends on undercooling below A_{e3} temperature, the following definition was assumed:

$$B_1 = a_4 \exp\left[-a_5\left(A_{e3} - T\right)\right] \tag{40}$$

B_2 time constant is responsible for the growth of the ferrite phase, so it was correlated with mobility of the interface and diffusion coefficient. Thus, it can be assumed that B_2 constant can be presented in the form of modified inverse Gauss function with a nose at the temperature of maximum transformation rate (a_7 coefficient). The following equation was proposed:

$$B_2 = \left\{ a_6 \exp\left[-\left(\frac{a_7 - T}{a_8} \right)^2 \right] \right\}^{-1} \tag{41}$$

With the application of such an approach it is possible to model metallurgical processes in real time, unlike in the case of approaches which use complicated computation methods. On the other hand, proposed model describes the phase transformation in variable temperature conditions (unlike simple model such as JMAK). Equation (38) is solved using finite difference method. The CONT model has one important advantage comparing to the JMAK. During solution of equation (38) the right hand side changes as a function of the temperature and the correction of X using equation (35) is not needed.

3.4. Mechanical properties

Various models of mechanical properties were introduced into the database. The first set contains conventional models developed in the second half of the XXth century. Beyond this, new models accounting for the effect of precipitation and dedicated to HSLA and AHSS grades were added to the base.

3.4.1. Conventional models

Conventional equations describing mechanical properties as function of the ferrite grain size and chemical composition were used as the default models in the VirtRoll database. The review of these models as well as coefficients for various steels can be found in (Lenard et al., 1999). Equations proposed by Hodgson and Gibbs (1992) were used as yield stress (Re) and ultimate tensile strength (Rm) models:

$$\mathrm{Re} = 62.6 + 26.1[\mathrm{Mn}] + 60.2[\mathrm{Si}] + 759[\mathrm{P}] + 212.9[\mathrm{Cu}] + 3286[\mathrm{N}] + \frac{19.7}{\sqrt{0.001 D_\alpha}} \tag{42}$$

$$\mathrm{Rm} = 164.9 + 634.7[\mathrm{C}] + 53.6[\mathrm{Mn}] + 99.7[\mathrm{Si}] + 652[\mathrm{P}] + 472.6[\mathrm{Ni}] + 3339[\mathrm{N}] + \frac{11}{\sqrt{0.001 D_\alpha}} \tag{43}$$

where: D_α – ferrite grain size.

3.4.2. Models accounting for the effect of precipitations

The new contribution of the present work is connected with accounting for precipitation during coiling. Physical simulations of cooling the strip in the coil and measurement of final mechanical properties were performed in the CEIT. Approximation of the results allowed to propose relation between mechanical properties and the coiling temperature, see Section 6.3. The model developed in the ArcelorMittal was another model implemented into the VirtRoll system database. This model uses the linear approach based on the summation of the contributions of solid solution (σ_{ss}), grain size(σ_{gs}), dislocations (σ_ρ), presence of secondary phases (σ_{MA}) and fine precipitation ($\Delta\sigma_{prec}$). The yield stress of the product is calculated as:

$$\mathrm{Re} = \sigma_0 + \sigma_{ss} + \sigma_{gs} + \sigma_\rho + \sigma_{MA} + \Delta\sigma_{prec} \tag{44}$$

The components of equation (44) account for the contribution of various factors are:

$$\sigma_{ss} = \sigma_0 + 32.3[\mathrm{Mn}] + 83.2[\mathrm{Si}] + 11[\mathrm{Mo}] + 354\left[\mathrm{N}_{free}\right]^{0.5} \tag{45}$$

$$\sigma_{gs} = 1.05\alpha M \mu \sqrt{b} \left[\sum_{2 \le \theta_i \le 15^\circ} f_i \sqrt{\theta_i} + \sqrt{\frac{\pi}{10}} \sum_{\theta_i \ge 15^\circ} f_i \right] d_{2^\circ}^{-\frac{1}{2}} \tag{46}$$

$$\sigma_\rho = \alpha M \mu b \sqrt{\rho} \tag{47}$$

$$\sigma_{MA} = 900 f_{MA} \tag{48}$$

$$10.8 \frac{f_v^{0.5}}{x} \ln\left(\frac{x}{6.125 \cdot 10^{-4}} \right) \tag{49}$$

where: M – Taylor factor, b – length of the Burgers vector, μ – shear modulus, ρ – dislocation density, f_i

– low ($2^o < \theta_l < 15^o$) and high ($\theta_i \geq 15^o$) angle boundary fractions, θ_i – misorientation angle, d_2^o - unit size considering the low angle misorientation criterion.

Details of the term accounting for the grain size are given in (Iza-Mendia & Gutiérrez, 2013). Average dislocation density in equation (47) is determined by the analysis of the Kernel Average Misorientation (KAM) by EBSD. KAM reflects the local misorientation gradients within a given region. For that purpose, the approach proposed in (Kubin et al., 2003) is adopted:

$$\rho = 2\frac{\mathrm{KAM}}{bu} \tag{50}$$

where: u – the length related to Kernel.

New model, which predicts the precipitation hardening effect ($\Delta\sigma_{prec}$) in coil for AHSS was developed by ArcelorMittal, as well. Calculation of the precipitation hardening effect ($\Delta\sigma_{prec}$) does not require information of precipitates size or density. The contribution of precipitation on the total stress depends on the Ti and Nb content. The effect of the thermal path is accounted for by integration with respect to time. Start temperature is calculated from the phase transformation model. Contribution of Nb and Ti to the yield stress is given by:

$$\Delta\sigma_{prec} = K_1 \exp\left[\frac{1}{K_2}\lg\left(\int_0^T \frac{dT}{K_4}\right)\right]^{K_3} \tag{51}$$

Coefficients $K_1 - K_3$ in equation (51) are different for Nb and Ti steels and they are given in table 2. Coefficient K_4 is defined as:

$$K_4 = \frac{10^{16}}{T}\exp\left(\frac{28000}{RT}\right) \tag{52}$$

Table 2. *Coefficients in equation (51) for various contents of Ti and Nb.*

steel	K_1	K_2	K_3
0.035%Nb	129.5	2	2
0.13%Ti	286	2	2

Selected results of calculations using equation (51) are presented in Section 6.3.

4. EXPERIMENTS

A variety of steel grades was investigated. Chemical compositions of these steels are given in Section 2.2. Three types of experiments were performed for identification of the models. Axisymmetric compression of cylindrical samples at various temperatures and strain rates was used to determine the coefficients in the flow stress models. Stress relaxation tests (Elwazri et al., 2004) were used for identification of the static part of the microstructure evolution model. Coefficients in the DRX and MDRX models were determined from the shape of the flow curves for low values of the Zener-Hollomon parameter. Strains at the peak stress and at the saturation stress were evaluated for various temperatures and strain rates and the results were approximated by equations in Section 3.2. Finally, dilatometric tests for various cooling rates were performed to supply data for the identification of the phase transformation models. For the HSLA and bainitic steels various temperatures and times between last deformation and beginning of transformation were used to supply data for different initial microstructures. Thermal cycles for all tests for the HSLA and bainitic steels are shown in figure 3. They include recrystallized (tests A and B) and not recrystallized (tests C and D) austenite.

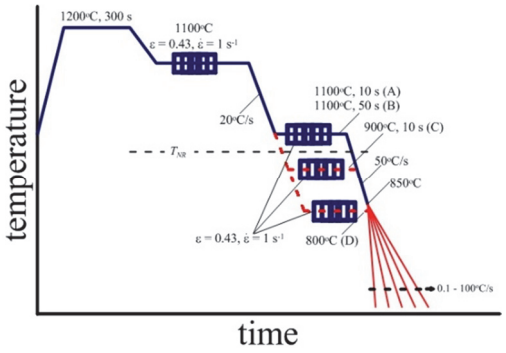

Fig. 3. *Temperature-deformation history for the bainitic steel and HSLA steel samples subjected to dilatometric tests.*

Following this, a set of experiments was performed to supply data for the validation and verification of the models. Physical simulations of the hot strip rolling were performed using plane strain compression (PSC) tests on the Gleeble 3800 thermomechanical simulator. In the PSC test a cuboid sample is compressed between two flat dies, see (Abad et al., 2001) for details. In this work the samples which measured 15×20×35 mm, were compressed in the dies with the width of 10 mm. The PSC test allows large plastic deformation and the state of strains is similar to that, which occurs in the flat rolling process. Therefore, the plane strain compression test has been for years used for physical simulation of rolling processes. Temperature and strain history can be easily reproduced in this test. Samples can be quenched after each deformation stage and micro-

structure can be investigated. However, problems with the interpretation of results of such physical simulation are connected with extensive inhomogeneity of strains and temperatures. Deformation and temperatures differ significantly at the cross section of the sample and, what is even more important, the shape coefficient Δ defined as the sample height-to-die width ratio changes during the test. FE simulation of the multi stage PSC test help to interpret the results, see (Pietrzyk et al., 2017) for details.

The tests for all materials were performed and the results were used for identification and validation of the models in the database. However, only selected tests for the HSLA and bainitic steels are presented in the paper.

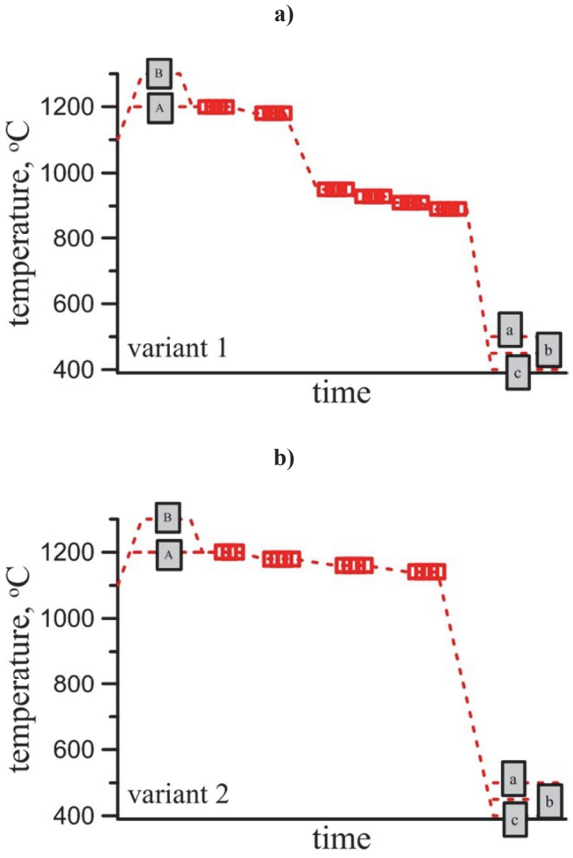

Fig. 4. *Schemes of deformation and heat treatment for bainitic steels investigated in the present work.*

Two variants of physical simulations were considered for bainitic steels, see (Pietrzyk et al., 2017) for details. Variant 1 is presented schematically in figure 4a. In this variant lower temperatures of deformation were applied. Variant 2 is presented schematically in figure 4b. This variant is characterised by higher temperatures of deformation. Quantitative data for both variants are given in table 3. Two preheating temperatures 1200°C and 1300°C were applied for each schedule, distinguished as A and B variants. Grain size prior to the first deformation (after soaking) was 67 μm for A and 191 μm for B. Cooling from the last deformation temperature to the holding temperature was at the rate of 20°C/s. Three holding temperatures (T_h) during cooling were used for each variant. Temperature T_h was 400, 450 and 500°C for cooling versions a, b and c, respectively.

Table 3. *Parameters of the investigated variants of physical simulations.*

parameter	Variant 1	Variant 2	Variant 3
Soaking temperature	1200°C (A), 1300°C (B)		1200°C
Soaking time	900 s	900 s	
Deformation temperature	1200°C	1200°C	1100°C
Strain; strain rate	0.35; 1 s^{-1}	0.35; 0.1 s^{-1}	0.4; 1 s^{-1}
Interpass time	15 s	10 s	15 s
Deformation temperature	1180°C	1180°C	1000°C
Strain; strain rate	0.25; 2 s^{-1}	0.3; 0.5 s^{-1}	0.4; 1 s^{-1}
Interpass time	40 s	10 s	15 s
Deformation temperature	950°C	1160°C	900°C
Strain; strain rate	0.2; 7 s^{-1}	0.3; 0.5 s^{-1}	0.4; 1 s^{-1}
Interpass time	5 s	10 s	0 s/10 s
Deformation temperature	930°C	1140°C	-
Strain; strain rate	0.15; 10 s^{-1}	0.2; 1 s^{-1}	-
Interpass time	4 s	32 s	-
Deformation temperature	910°C	-	-
Strain; strain rate	0.1; 10 s^{-1}	-	-
Interpass time	3 s	-	-
Deformation temperature	890°C		-
Strain; strain rate	0.1; 10 s^{-1}		-
Interpass time	19.5 s		-
Holding temperature	T_h		
Holding time	5400 s		

Schematic illustration of the tests performed for the HSLA steels is shown in figure 5. In this variant the last temperature was 900°C and cooling begun either right after deformation (no recrystallization) or 10 s after deformation (full recrystallization). Quantitative data for the variant 3 are given in table 3.

Grain size prior to the first deformation (after soaking) was 75 μm. Cooling from the last deformation temperature to the holding temperature was at the rate of 20°C/s. Different holding temperatures (T_h = 400 ÷ 700°C) representing cooling in the coil were used for each variant.

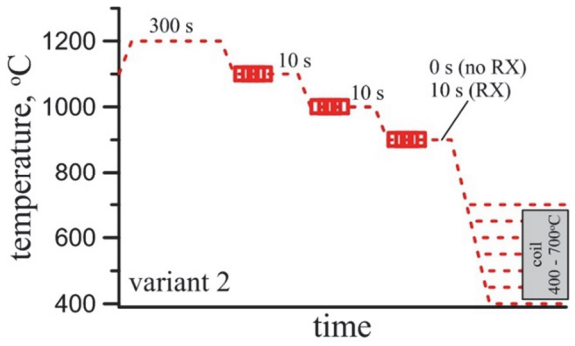

Fig. 5. *Schemes of deformation and heat treatment for HSLA steels investigated in the present work.*

After each test for the HSLA and bainitic steels the samples were quenched and the microstructure characterization, as well as mechanical properties measurement, were performed. Phase composition at the centre of the sample was evaluated and was used to validate the phase transformation model.

Analysis of strains in the PSC tests was performed first and strong inhomogeneities were observed. Different distributions of strains were obtained at different stages of deformation, depending on the shape coefficient Δ. In the variant 1 height of the sample in subsequent staged was 15; 11.08; 8.93; 7.52; 6.61 and 6.06 mm what gave shape coefficients Δ = 1.5; 1.108; 0.893; 0.752; 0.661; 0.606 respectively for stages 1 – 6. This change of the shape coefficient involves changes of the inhomogeneity of deformation. The general approach followed by the scientists was to investigate the material in the centre of the sample, assuming that strains and temperatures at that location are close to the nominal values. The nominal temperature is assumed equal to the initial one, and the nominal strain is calculated as:

$$\varepsilon_h = \frac{2}{\sqrt{3}} \ln\left(\frac{h_i}{h_{i+1}}\right) \tag{53}$$

where: h_i – initial height of the sample, h_{i+1} – final height of the sample after deformation, i – pass number.

Strains calculated by the FE code in the centre of the sample were much higher than nominal strains calculated from equation (53) (figure 6), which are generally used to calculate recrystallization kinetics and grain size. It means that classical interpretation of the tests results may introduce errors.

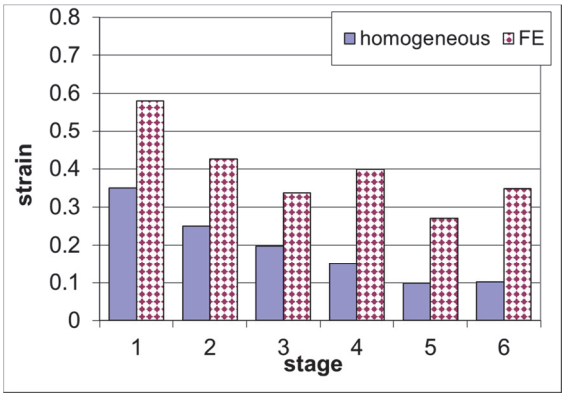

Fig. 6. *Comparison of the homogeneous strains ε_h with strains at the centre of the sample calculated by the FE code for variant 1 in* ***Fig. 4****b.*

5. INVERSE APPROACH

Inverse analysis was used to determine the material parameters in the models corrected against the effect of various disturbances in the tests. In the plastometric tests it is the effect of friction and deformation heating. Since automatic temperature control system is used in the tests, the latter effect is particularly important. In the inverse analysis the temperature measured by the thermocouple welded to the sample is introduced as a Dirichlet boundary condition in the FE code. In the dilatometric tests the effect of recalescence has to be eliminated.

5.1. Basic principles of the approach

The inverse algorithm described by Szeliga et al. (2006) and tested and validated by Szeliga and Pietrzyk (2007) was used. In this algorithm the inverse problem is transferred into the optimization task. Thus, the coefficients in the models were determined using optimization techniques, as it is shown schematically in figure 7. In this figure **a** is the vector of coefficients in the model, **p** is the vector of parameters of experiments and **d** is the vector of outputs of the model, which are the parameters measured in the experiment. In plastometric tests **p** is composed of temperatures and strain rates in the tests and **d** is composed of measured forces. In dilatometric tests **p** is composed of cooling rates in the tests and **d** is composed of measured start and end temperatures of transformations as well as phase volume fractions. The quadratic norm of the error between measured and calculated output parameters in the tests was used as the objective function:

– For the flow stress model

$$\Phi = \sqrt{\frac{1}{Nt}\sum_{i=1}^{Nt}\left[\frac{1}{Ns}\sum_{j=1}^{Ns}\left(\frac{F_{ij}^{m}-F_{ij}^{c}}{F_{ij}^{m}}\right)^{2}\right]} \quad (54)$$

– For the phase transformation model

$$\Phi = \sqrt{\frac{1}{Ncr}\sum_{i=1}^{Ncr}\left[\frac{1}{Ntc}\sum_{j=1}^{Ntc}\left(\frac{T_{ij}^{m}-T_{ij}^{c}}{T_{ij}^{m}}\right)^{2}+\frac{1}{Np}\sum_{j=1}^{Ns}\left(\frac{V_{ij}^{m}-V_{ij}^{c}}{V_{ij}^{m}}\right)^{2}\right]} \quad (55)$$

where: Nt – number of plastometric tests, Ns – number of load measurement sampling points in one test, F_{ij}^{m}, F_{ij}^{c} – measured and calculated force, Ncr – number of cooling rates in dilatometric tests, Ntc – number of characteristic temperatures measured for one cooling rate, Np – number of phases, T_{ij}^{m}, T_{ij}^{c} – measured and calculated start and end temperatures for phase transformations, V_{ij}^{m}, V_{ij}^{c} – measured and calculated volume fractions of phases.

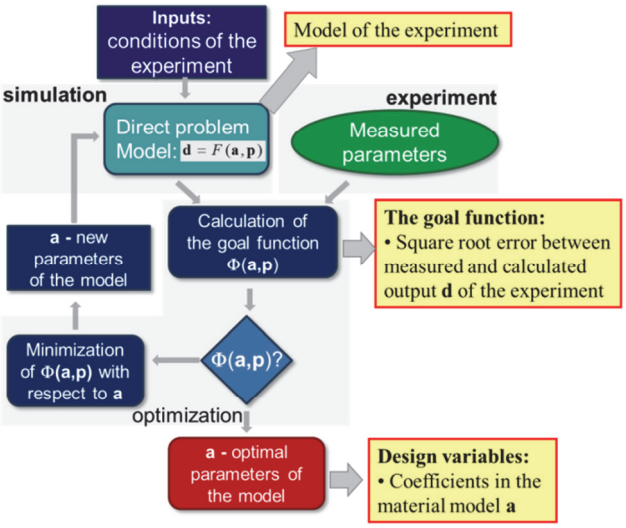

Fig. 7. *Flow chart of the inverse solution based on optimization.*

Table 4. *Coefficients in the Hensel-Spittel flow stress equation (2).*

steel	A	n	q	m	β
S401	2506.3	0.40597	0.55992	0.098814	0.002523
S403	2509.6	0.40052	0.55181	0.09905	0.002518
S404	2378.2	0.40034	0.53519	0.097066	0.002462
S405	6882.4	0.32626	0.44235	0.07694	0.003483
S406	10539	0.43527	0.78879	0.11177	0.003549
S407	50570	0.95395	2.0559	0.10553	0.004108
S447-S449	6882.4	0.32626	0.44235	0.07694	0.003483
AHSS9	4872.1	0.56658	1.1377	0.13805	0.002729
AHSS10	4998.3	0.31122	0.56106	0.11603	0.003126
AHSS11	4545.3	0.31194	0.54148	0.11587	0.003061
AHSS12	4382.4	0.25995	0.34619	0.11564	0.003089

5.2. Identification of material models

All models presented in Chapter 3 contain coefficients, which were identified on the basis of the experimental tests. As it has been mentioned, plastometric tests, stress relaxation tests and dilatometric tests were subsequently used for identification of the flow stress, microstructure evolution and phase transformation models. The coefficients in the flow stress equations (1) - (6) obtained for the investigated steels are given in tables 4-7.

The coefficients of the microstructure evolution models were determined on the basis of experiments for the majority of steels investigated in this work. Some of the coefficients were taken from the literature. Stress relaxation tests were used to determine coefficients in the static recrystallization model. Interpretation of these tests is described in (Smith et al., 2006) and the values of the coefficients are given in Table 8. Coefficients in equation (12) describing grain size after static recrystallization for the DP steels S447, S448 and S449 were taken from the literature (Kuziak & Pietrzyk, 2016).

Coefficients in equations describing the dynamic recrystallization were determined on the basis of the analysis of the flow curves. These coefficients are given in table 9 and table 10 for the DRX and the MDRX, respectively. Coefficients in equations (24) and (25) describing grain size after dynamic and metadynamic recrystallization for the HSLA steels S401, S403 and S404 were taken from the literature (Abad et al., 2001). Finally, coefficients in equation (14) describing grain growth are given in Table 11.

In a majority of steels investigated in the present work multiphase structures are required and the ferrite grain size is of minor importance. Therefore, the model based on equation (27) was used for all steels and the coefficients were taken from the literature (Hodgson & Gibbs, 1992). Values of these coefficients are given in table 12.

The coefficients in the phase transformation models were determined by the inverse analysis of the dilatometric tests. The inverse algorithm described Pietrzyk and Kuziak (2012) was applied. All the tests were performed within this work for the investigated four groups of steels. In the case of the HSLA steels and bainitic steels four different thermal cycles between last deformation and beginning of transformation were applied, see figure 3. Inverse analysis have shown that the time after deformation

Table 5. *Coefficients in the flow stress equation (3).*

steel	K	Q	n	m	K_{sat}	Q_{sat}	W
S401	8.9004	2987.9	0.35586	0.098892	0.20517	6563.8	0.84624
S403	11.159	2775.1	0.36997	0.099419	0.22532	6479.5	0.9513
S404	12.475	2654.6	0.37527	0.097314	0.26277	6341.2	0.98103
S405	11.041	2828.1	0.3614	0.082657	0.54491	6140.5	4.8414
S406	5.3887	3966.1	0.37585	0.11121	0.22373	7208.3	2.0923
S407	12.601	5402.9	1.4358	0.11422	0.42871	6311.6	7.0754
S447-S449	11.041	2828.1	0.3614	0.082657	0.54491	6140.5	4.8414
AHSS9	38.628	1047.6	0.41819	0.13785	0.49533	6057.8	3.2179
AHSS10	45.706	164.85	0.17743	0.13251	0.90192	5474.7	6.451
AHSS11	69.291	241.71	0.39393	0.13499	1.1294	5146.2	6.8212
AHSS12	23.622	1669.3	0.30189	0.14004	1.13	5237.1	4.283

Table 6. *Coefficients in the flow stress equation (4).*

	S401	S403	S404	S408	S405	S406	S407	S447-S449	AHSS9	AHSS10	AHSS11	AHSS12
A_0	$6.462\cdot10^{11}$	$6.462\cdot10^{11}$	$8.412\cdot10^{11}$	$1.0419\cdot10^{12}$	$1.008\cdot10^{13}$	$1.75E\cdot10^{12}$	$1.11\cdot10^{12}$	$3.35\cdot10^{22}$	$1.926\cdot10^{11}$	$1.01\cdot10^{11}$	$5.77\cdot10^{10}$	$1.346\cdot10^{11}$
n_0	129	128.73	150.17	180.34	2037.3	264	164	9.50656	326.36	398.98	27.506	224.25
α_0	0.0456	0.04562	0.044491	0.043623	0.085353	0.0.33	0.267	$2.24\cdot10^{-03}$	0.090604	0.054547	0.041652	0.043077
A_{sse}	$1.77\cdot10^{14}$	$1.769\cdot10^{14}$	$1.675\cdot10^{14}$	$1.518\cdot10^{14}$	$1.963\cdot10^{14}$	$1.22\cdot10^{14}$	$1.19\cdot10^{14}$	$2.18\cdot10^{+12}$	$3.553\cdot10^{13}$	$4.681\cdot10^{13}$	$4.176\cdot10^{13}$	$3.364\cdot10^{13}$
n_{sse}	7.49	7.493	7.7134	7.7996	2.6	6.17	4.90	7.703552	6.2294	4.989	5.0817	5.0258
α_{sse}	0.008.69	0.008685	0.0085675	0.0085866	0.027444	0.007.05	0.00847	$5.19\cdot10^{-03}$	0.010178	0.010835	0.01144	0.010093
A_{ss}	$3.83\cdot10^{10}$	$3.827\cdot10^{10}$	$5.292\cdot10^{10}$	$6.685\cdot10^{10}$	$9.976\cdot10^{10}$	$1.40\cdot10^{11}$	$2.85\cdot10^{10}$	$1.23\cdot10^{21}$	$7.326\cdot10^{10}$	$1.926\cdot10^{10}$	$5.21\cdot10^{10}$	$5.062\cdot10^{10}$
n_{ss}	5.29E	5.2891	4.4988	3.7521	6.2059	3.78	6.62	6.679322	22.777	9.0015	4.5373	8.5759
α_{ss}	0.0.96	0.029643	0.031397	0.035943	0.055978	0.0344	0.0332	$3.39\cdot10^{-4}$	0.02174	0.0276	0.037457	0.024455
q_1	1.20	1.1996	1.1311	1.1497	0.5465	1.04	0.658	0.774121	1.4238	0.56922	0.66294	0.73754
q_2	$1.65\cdot10^{-11}$	$1.65\cdot10^{-11}$	$1.65\cdot10^{-11}$	$1.65\cdot10^{-11}$	$1.65\cdot10^{-11}$	$1.65\cdot10^{-11}$	$1.65\cdot10^{-11}$	281929.6	$1.65\cdot10^{-11}$	$1.65\cdot10^{-11}$	$1.65\cdot10^{-11}$	$1.65\cdot10^{-11}$
C_c	0.0346	0.034595	0.033395	0.034615	0.011525	0.00891	0.0224	$2.73\cdot10^{-03}$	0.012228	0.022479	0.025842	0.009668
N_c	0.1	0.10031	0.097578	0.091752	0.087781	0.0767	0.0930	0.295522	0.088561	0.10122	0.10451	0.1028
C_x	0.00393	0.003928	0.0037058	0.0034455	0.0057443	0.00350	0.00577	$3.90\cdot10^{-03}$	0.0061826	0.0047986	0.0039132	0.004618
N_x	0.239	0.23897	0.24659	0.26319	0.20676	0.260	0.266	0.31971	0.21637	0.23026	0.2341	0.24359
Q_{def}	375000	374980	374150	374550	448810	382000	372000	$8.53\cdot10^{-12}$	401830	383530	385880	384870

Table 7. *Coefficients in the flow stress equation (6).*

	S401	S403	S404	S408	S405	S406	S407	S447-S449	AHSS9	AHSS10	AHSS11	AHSS12
σ_0	10	10	10	5.3359	9.5982	11.528	0.23759	9.5982	2.7505	0.26145	7.6736	0.39826
C_c	0.0005056	0.0005056	0.0005056	0.003398	0.000924	0.0009355	0.0015447	0.0009239	0.092808	0.045115	0.021354	0.044724
C_x	0.0002809	0.0002809	0.0002809	$2.955\cdot10^{-6}$	$7.865\cdot10^{-6}$	$3.482\cdot10^{-4}$	$3.3202\cdot10^{-4}$	$7.865\cdot10^{-6}$	$1.41\cdot10^{-5}$	$3.123\cdot10^{-6}$	$6.6138\cdot10^{-7}$	$7.661\cdot10^{-6}$
N_1	0.2	0.2	0.2	0.0040813	0.13575	0.22522	0.18564	0.13575	0.004555	0.001176	0.01558	0.0087965
N_2	0.25	0.25	0.25	0.32228	0.28718	0.23064	0.2104	0.28718	0.28969	0.37014	0.4276	0.36187
A_{ss}	0.012	0.012	0.012	0.022005	0.012986	0.0090076	0.011347	0.012986	0.013302	0.009162	0.0092904	0.0084398
n_{ss}	$5.42\cdot10^{11}$	$3.92\cdot10^{11}$	$3.92\cdot10^{11}$	$2.248\cdot10^{13}$	$5.607\cdot10^{10}$	$7.951\cdot10^{11}$	$1.213\cdot10^{11}$	$5.607\cdot10^{10}$	$2.47\cdot10^{12}$	$7.4\cdot10^{12}$	$6.185\cdot10^{12}$	$6.738\cdot10^{12}$
α_{ss}	5	5	5	3.2755	3.8734	3.8295	3.8512	3.8734	5.1801	5.8676	5.725	6.2423
a_β	12.3	12.5	12.5	6.0584	4.9485	19.34	5.4017	4.9485	4.056	7.2839	9.4017	8.3093
b_β	0.59	0.59	0.59	0.015606	0.0037341	1.0276	0.0075108	0.0037341	0.066488	0.014555	0.17805	0.14493
q_1	0.15	0.15	0.15	0.37822	0.037658	0.035954	0.055562	0.037658	0.082502	0.26624	0.19316	0.15
q_2	0.26	0.26	0.26	0.26	1.4965	0.38019	0.67784	1.4965	0.34172	0.19869	0.12565	0.26
C	0.15	0.15	0.15	0.15	0.32329	0.16315	0.2092	0.32329	0.41801	0.24455	0.27352	0.29453
Q_{def}	325000	325000	325000	325000	314440	314440	314440	314440	385330	355190	342470	357760

Table 8. *Coefficients in microstructure evolution equations for static recrystallization.*

steel	n	A	a_1	a_2	a_3	Q_{SRX}	B	b_1	b_2	b_3	Q_{DSRX}
S401	1	$7.42\cdot10^{-11}$	5.6	0.53	1	180000	1.4	1	0	0.56	0
S403	1	$7.42\cdot10^{-11}$	5.6	0.53	1	180000	1.4	1	0	0.56	0
S404	1	$7.42\cdot10^{-11}$	5.6	0.53	1	180000	1.4	1	0	0.56	0
S405	2.18	$1.69\cdot10^{-11}$	1.62	0.3	0.787	227776	14.43	0.962	0	0.563	28638
S406	1.53	$1.738\cdot10^{-11}$	3.6	0.3	0.7075	205000	1.487	0.055	0.08	0.88	8172
S407	2.18	$1.806\cdot10^{-11}$	2.181	0.345	0.545	258704	7.623	0.936	0.117	0.664	26144
S447	2.182	$18.06\cdot10^{-11}$	2.181	0.345	0.545	258704	63.7	0.739	0.05	0.2	29324
S448	1.783	$1.738\cdot10^{-11}$	3.269	0.3	0.7075	207186	63.7	0.739	0.05	0.2	29324
S449	2.182	$1.806\cdot10^{-11}$	2.181	0.345	0.545	258704	63.7	0.739	0.05	0.2	29324
AHSS9	0.8	7.40E-14	-1.679	-0.402	2	218630	63.71	-0.739	-0.05	0.2	29324
AHSS10	0.8	7.4E-14	-1.679	-0.402	2	218630	63.71	-0.739	-0.05	0.2	29324
AHSS11	0.8	7.4E-14	-1.679	-0.402	2	218630	63.71	-0.739	-0.05	0.2	29324
AHSS12	0.8	7.4E-14	-1.679	-0.402	2	218630	63.71	-0.739	-0.05	0.2	29324

Table 9. *Coefficients in microstructural equations for dynamic recrystallization.*

steel	p_1	p_2	p_3	p_4	p_5	p_6	p_7	p_8	p_9	p_{10}
S401	$5.0562\cdot10^{-4}$	0.15	0.0088	$2.809\cdot10^{-4}$	0.26	0.36187	4.60517	1.5	$1.6\cdot10^{4}$	0.23
S403	$5.0562\cdot10^{-4}$	0.15	0.0088	$2.809\cdot10^{-4}$	0.26	0.36187	4.60517	1.5	$1.6\cdot10^{4}$	0.23
S404	$5.0562\cdot10^{-4}$	0.15	0.0088	$2.809\cdot10^{-4}$	0.26	0.36187	4.60517	1.5	$1.6\cdot10^{4}$	0.23
S405	$11.28\cdot10^{-4}$	0.1629	0.1774	$4.846\cdot10^{-3}$	0.1326	0.1677	1.71	1.5	$2.293\cdot10^{4}$	0.2499
S406	$5.377\cdot10^{-4}$	0.355	0.176	$5.48\cdot10^{-3}$	0.3702	0.1156	1.5	1.5	$2.229\cdot10^{4}$	0.3289
S407	$3.7\cdot10^{-4}$	0.3434	0.1914	$8.76\cdot10^{-3}$	0.3819	0.1939	1.5	1.5	$1.737\cdot10^{4}$	0.325
S447	$1.031\cdot10^{-4}$	0.5	0.2226	$1.737\cdot10^{-3}$	0.5	0.2472	2.092	1.8	416.68	0.13
S448	$1.343\cdot10^{-4}$	0.5	0.2231	$0.215\cdot10^{-3}$	0.5	0.2499	2.612	1.8	416.68	0.13
S449	1.031·10-4	0.5	0.2226	$1.737\cdot10^{-3}$	0.5	0.2472	2.092	1.8	416.68	0.13
AHSS9	0.001657	0.147	0.155	0.000291	0.26	0.25	0.639	1.5	16000	0.23
AHSS10	0.001657	0.147	0.155	0.000291	0.26	0.25	0.639	1.5	16000	0.23
AHSS11	0.001605	0.147	0.155	0.000282	0.26	0.25	0.639	1.5	16000	0.23
AHSS12	0.001605	0.147	0.155	0.000282	0.26	0.25	0.639	1.5	16000	0.23

Table 10. *Coefficients in microstructural equations for metadynamic recrystallization.*

steel	q_1	q_2	q_3	Q_{MDRX}	q_4	q_5
S401	1	$3.1\cdot10^{-8}$	0.6	170000	$2.6\cdot10^{-4}$	0.23
S403	1	$3.1\cdot10^{-8}$	0.6	170000	$2.6\cdot10^{-4}$	0.23
S404	1	$3.1\cdot10^{-8}$	0.6	170000	$2.6\cdot10^{-4}$	0.23
S405	1.552	0.059	0.9005	301735	$2.293\cdot10^{4}$	0.2499
S406	2.275	1.714	0.8088	239122	$2.229\cdot10^{4}$	0.3289
S407	2.068	0.002	1.063	386264	$1.737\cdot10^{4}$	0.325
S447	1.447	0.024	0.8398	264135	17370	0.325
S448	1.26	$1.089\cdot10^{-6}$	0.3217	240904	22290	0.3289
S449	1.447	0.0238	0.8398	264136	17370	0.325

Table 11. *Coefficients in the grain growth equations*

steel	s	K	Q_{GROWTH}
S401	7.19	$2.67\cdot10^{22}$	349805
S403	7.19	$2.67\cdot10^{22}$	349805
S404	7.19	$2.67\cdot10^{22}$	349805
S405	7.19	$2.67\cdot10^{22}$	349805
S406	7.36	$9.48\cdot10^{16}$	187667
S407	8	$8.575\cdot10^{22}$	361948
S447	7.19	$2.67\cdot10^{22}$	349805
S448	7.19	$2.67\cdot10^{22}$	349805
S449	7.19	$2.67\cdot10^{22}$	349805

Table 12. *Coefficients in equation (27) describing ferrite grain size in steels with $D_{eq} < 0.35\%$.*

f_0	f_1	f_2	f_3	f_4	f_5
-0.4	6.37	24.2	-59	22	0.015

at 1100°C has small influence on the kinetics of transformation and similar coefficients were obtained for the tests A and B. In the test D deformation was below the A_{e3} temperature and these data were not used in the model identification. Coefficients in the phase transformation models obtained from the inverse analysis for all steels and for all thermal cycles are given in table 13.

Table 13. *Coefficients in the phase transformation JMAK based model – equations (29) - (31).*

steel	a_4	a_5	a_6	a_7	a_8	a_9	a_{10}	a_{11}	a_{12}	a_{13}	a_{14}	a_{15}	a_{16}	a_{17}	a_{18}	a_{19}	a_{20}	a_{21}	a_{22}	a_{23}	a_{24}	a_{25}	a_{26}
S401A	3.0	0.098	196.8	29.5	1.47	4.37	61.6	1.566	0	0	0	4.172	1.236	2551	63.1	3.5	717.9	0.94	4.638	3.655	0.287	390.7	10.82
S401B	3.0	0.098	196.8	29.5	1.47	4.37	61.6	1.566	0	0	0	4.172	1.236	2551	63.1	3.5	717.9	0.94	4.638	3.655	0.287	390.7	10.82
S401C	1.87	0.405	192.1	45.9	1.66	4.86	57.5	1.604	0	0	0	24.17	2.0	2523	56.9	3.22	685.9	1.42	5.525	4.586	0.208	390.7	10.82
S403A	2.23	0.627	251.0	44.0	1.72	6.47	23.2	0.054	0	0	0	19.31	1.986	2539	55.7	3.38	622.1	5.34	21.83	8.506	1.838	411.5	12.19
S403B	2.23	0.627	251.0	44.0	1.72	6.47	23.2	0.054	0	0	0	19.31	1.986	2539	55.7	3.38	622.1	5.34	21.83	8.506	1.838	411.5	12.19
S403C	2.03	0.542	270.7	52.5	1.52	3.21	16.0	0.113	0	0	0	19.31	1.986	2784	54.8	3.4	602.6	5.37	21.12	8.467	2.108	376.7	16.96
S404A	2.33	0.644	272.8	44.8	1.68	6.69	24.3	0.059	0	0	0	19.31	1.986	2775	55.8	3.5	625.3	5.36	23.06	8.709	1.675	411.1	12.85
S404B	2.33	0.644	272.8	44.8	1.68	6.69	24.3	0.059	0	0	0	19.31	1.986	2775	55.8	3.5	625.3	5.36	23.06	8.709	1.675	411.1	12.85
S404C	2.59	0.632	290.5	49.4	1.51	8.58	8.05	0.0738	0	0	0	19.31	1.986	3040	57.1	3.5	622.6	5.47	23.69	0.018	1.739	329.5	24.41
S405A	2.86	0.084	194.1	18.5	1.33	1515	69.5	2.294	0	0	0	1.856	0.791	2528	70.0	3.35	737.5	2.62	2.199	3.094	1.245	390.7	10.82
S405B	1.86	0.089	186.4	21.8	1.14	1525	70.5	2.194	0	0	0	1.856	0.791	2536	69.8	3.43	735.5	2.62	2.199	3.094	1.245	390.7	10.82
S405C	2.03	0.060	168.8	46.1	1.93	1526	68.4	2.32	0	0	0	1.856	0.791	2593	70.1	3.35	732.0	2.62	2.199	3.094	1.245	395.7	10.82
S405D	2.29	0.085	182.3	29.1	1.68	1525	68.5	2.326	0	0	0	1.856	0.791	48.95	24.2	1.28	729.6	4.49	2.481	0.532	2.565	397.7	10.82
S406A	2.73	0.061	206.2	17.2	1.0	1515	69.5	2.294	0	0	0	0.056	0.381	19.37	25.3	1.22	726.1	2.62	2.199	3.094	1.245	400.0	10.82
S406B	2.72	0.061	206.3	16.9	1.0	1515	89.5	2.294	0	0	0	1.856	0.791	19.84	2560	1.26	717.7	2.55	2.332	5.188	1.153	407.7	10.82
S406C	2.61	0.080	150.3	23.8	1.59	1515	69.5	2.294	0	0	0	1.856	0.791	20.04	25.7	1.28	715.0	4.23	2.607	0.54	2.511	407.7	10.82
S406D	2.70	0.082	167.8	24.5	1.64	1515	89.5	2.294	0	0	0	1.856	0.791	20.35	25.5	1.35	704.1	4.33	2.481	0.532	2.565	407.7	10.82
S407A	2.46	0.036	219.5	58.9	2.41	1525	88.5	2.326	0	0	0	1.856	0.791	55.19	24.2	1.28	737.7	4.69	2.678	0.753	2.678	400.7	10.82
S407B	2.59	0.023	206.3	72.8	2.51	1525	88.5	2.326	0	0	0	1.856	0.791	56.2	24.2	1.38	737.3	4.69	2.678	0.957	2.677	403.7	10.82
S407C	1.74	0.057	154.0	75.3	3.0	1525	88.5	2.326	0	0	0	1.856	0.791	56.09	23.9	1.37	734.2	4.75	2.655	1.401	2.678	406.8	10.82
S407D	2.08	0.105	155.3	35.2	2.28	1525	88.5	2.326	0	0	0	1.856	0.791	56.9	22.4	1.45	720.0	4.82	2.655	1.403	2.686	394.3	0.08
S447	1.71	8.738	180.2	75.6	3.0	3.318	46.6	1.606	0	0	0	0.089	0.791	42.65	25.2	1.78	711.2	1.99	1.553	0.413	3.064	437.3	0.083
S448	1.71	8.738	180.2	75.6	3.0	3.318	46.6	1.606	0	0	0	0.089	0.791	42.65	25.2	1.78	711.2	1.99	1.553	0.413	3.064	437.3	0.083
S449	1.71	8.738	180.2	75.6	3.0	3.318	46.6	1.606	0	0	0	0.089	0.791	42.65	25.2	1.78	711.2	1.99	1.553	0.413	3.064	437.3	0.083
AHSS9	1.31	3.482	226.3	38.8	1.70	97.2	3.78	0.356	0	0	0	1.667	0.128	1562.6	64.5	3.12	699.4	1.48	0.575	4.	1.988	413.7	4.694
AHSS10	2.76	0.133	252.5	40.1	2.42	129.1	5.88	0.038	0	0	0	1.667	0.128	1581.7	64.5	3.31	658.5	1.99	0.553	4.521	1.776	413.7	4.694
AHSS11	1.32	5.227	217.9	44.2	1.94	9.37	11.8	0.0002	0	0	0	1.78	0.112	1842.7	64.6	3.24	690.9	2.09	0.584	4.959	3.33	420.6	7.35
AHSS12	1.02	6.331	252.9	42.3	1.37	13.33	12.1	0.0004	0	0	0	1.78	0.112	1898.6	65.0	3.28	687.2	1.84	0.822	4.243	2.33	414.6	7.35

6. NUMERICAL TESTS OF THE MODELS AND DISCUSSION

The contribution of this work is discussed under the two aspects. The first is connected with the specific functionalities of the developed database. The second includes new aspects of modelling of materials investigated in the paper.

6.1. Functionalities of the database

The database itself is not a modern solution while it is based on the well-known object oriented database management system MongoDB. However, the most innovative part is related to the architecture of the whole system which includes the following elements using information stored in the database:

- VirtRoll frontend and backend – the database delivers records on materials, their properties and chemical compositions, devices and already designed processes as well as optimization and sensitivity analysis methods with their parameters. In this part of the system created database is the most integral part.
- Scalarm platform as middleware – this element of the whole solution keeps information on the samples of the computational space used by sensitivity analysis and optimization methods. The data are passed usually one way from the database to Scalarm platform as the information on how to realize calculations.
- FEM based module for calculations on the HPC side – mainly the records related to configuration of devices in particular designs are delivered to this module of the system.
- External EDA knowledge base delivering data on materials and models – the exchange between EDA knowledge base and database presented in this paper can be realized two ways i.e. EDA can deliver information on material models and their parameters, while the proposed database feeds EDA with data on material properties and chemical composition.

Rich communication interfaces implemented for the purposes of data exchange between created database and other external systems offer functionality, which can be easily extended. Thus, the scalability of proposed solution is high and allows for further development.

6.2. Validation and verification of the models

Numerical simulation of the PSC tests were used to validate and verify the models. Authors' FE code (Pietrzyk, 2000) was used in simulations. The tests supplied the data for verification of the microstructure evolution model, as well as for the analysis of the effect of coiling temperature on the mechanical properties of products. Evaluation of the error in interpretation of experimental data connected with neglecting strain inhomogeneity in the PSC test was the first objective of simulations. Application of the simulations to predict microstructure of steels after the process and validation of the microstructure evolution model was performed next.

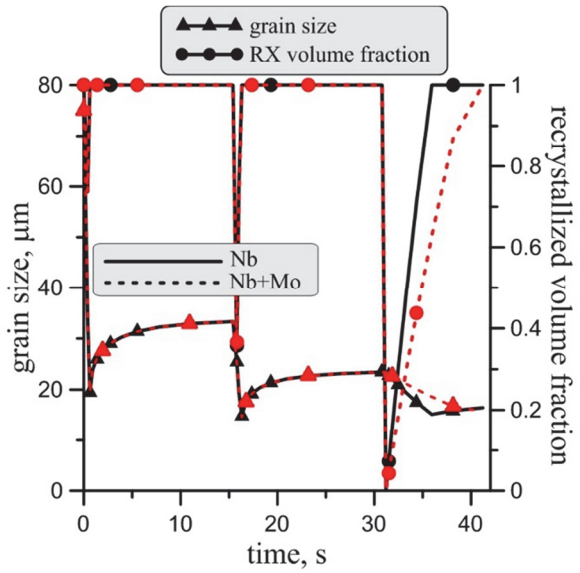

Fig. 8. *Calculated grain size and recrystallized volume fraction changes during the test in* ***Fig. 5*** *for the Nb (S401) and Nb+Mo (S403) steels.*

Numerical simulations were carried out for all the performed tests and for all the investigated steels. Due to space limit results for the HSLA steels only are presented in this Section. Some of the results of simulations of grain size evolution during the tests for the bainitic steels, as well changes of the recrystallized volume fraction for these steels, are shown and discussed in (Pietrzyk et al., 2017). Calculated grain size and recrystallized volume fraction changes during the test in figure 5 are shown in figure 8. It is seen that at the passes 1 and 2 the difference between the two steels is negligible. After the last pass at 800°C recrystallization is slower for the Nb+Mo steel (S403). Calculated final grain size is comparable for both steels about 21 μm and similar value was measured in the experiments.

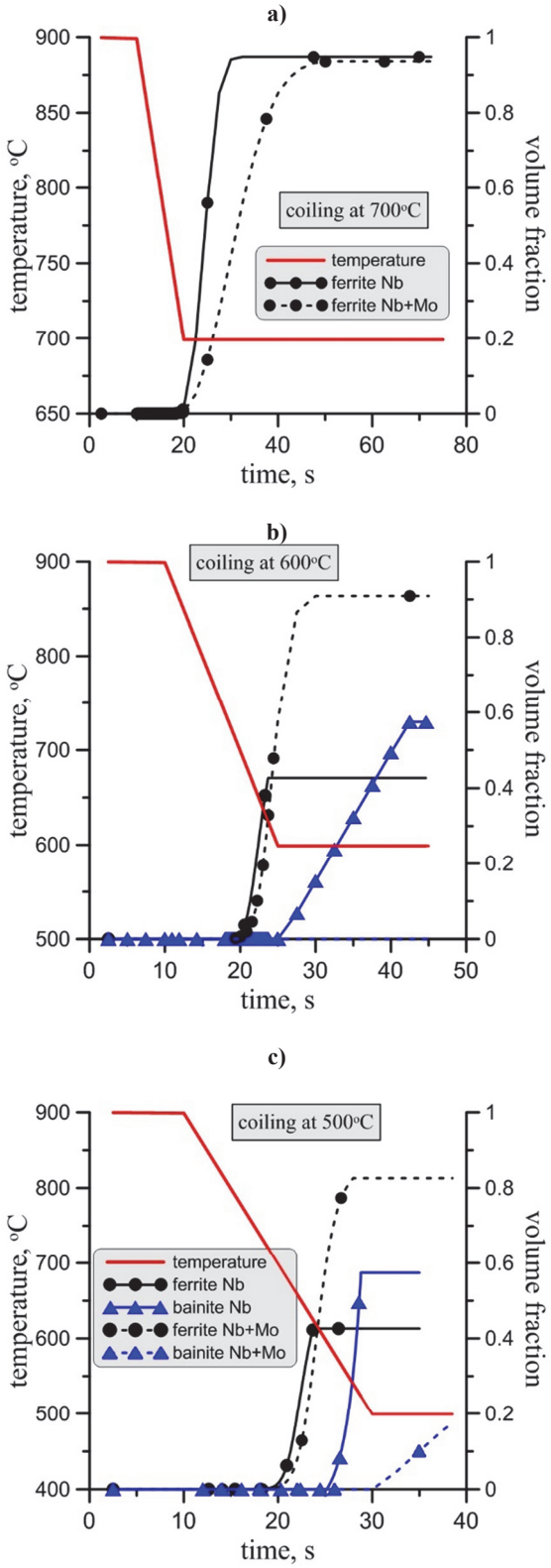

Fig. 9. *Kinetics of transformation after cycles in figure 5 with the coiling temperatures of 700°C (a), 600°C (b) and 500°C (c), for recrystallized austenite (meaning of symbols is the same in all plots).*

In order to find the relationship between microstructure and mechanical properties, different coiling temperatures and holding times after last transformation were applied. Coiling was reproduced by holding the samples for 90 min in the constant tem-

perature followed by slow cooling in the furnace at 1ºC/s to the room temperature. Numerical simulations of this sequence were performed and the results are presented in figure 9. It is seen in this figure that kinetics of the ferrite transformation is faster for the Nb steel and bainite start temperature is much higher for this steel. Results of calculations were confronted with the microstructure observed in the experiments.

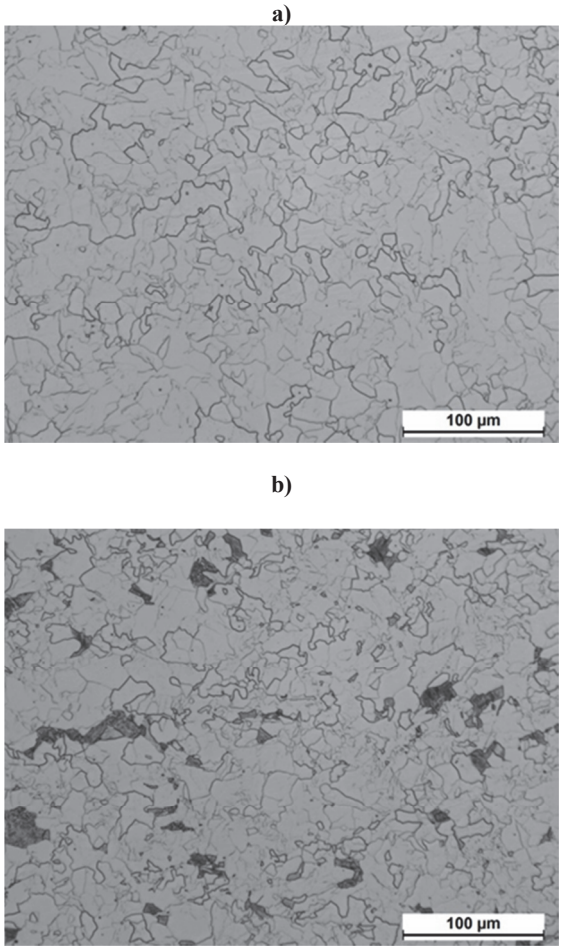

Fig. 10. *Optical micrographs of microstructures corresponding to Nb steel (S401) at the coiling temperatures 700ºC (a) and 600°C (b).*

In figure 10 the optical micrographs of the specimens of Nb microalloyed steel (S401) coiled at 700 and 600ºC are shown. A gradual shift from high temperature phases such as Polygonal Ferrite (PF) to lower temperature phases, such as Quasipolygonal Ferrite (QF) and Granular Ferrite (GF) was observed when decreasing the coiling temperature. Mechanical properties were measured for each sample in CEIT and they were approximated as functions of the coiling temperature, see next section. In figure 11 FEG-SEM micrographs corresponding to Nb steel (S401), obtained after different coiling temperatures are presented. In brief, a key point is that in Nb microalloyed steel, when a high coiling temperature is applied, the microstructure is composed by polygonal ferrite (PF) and pearlite (see figure 11a). A combination between quasipolygonal ferrite (QF) and granular ferrite (GF) is formed when coiling temperature decreases (see figure 11b and c).

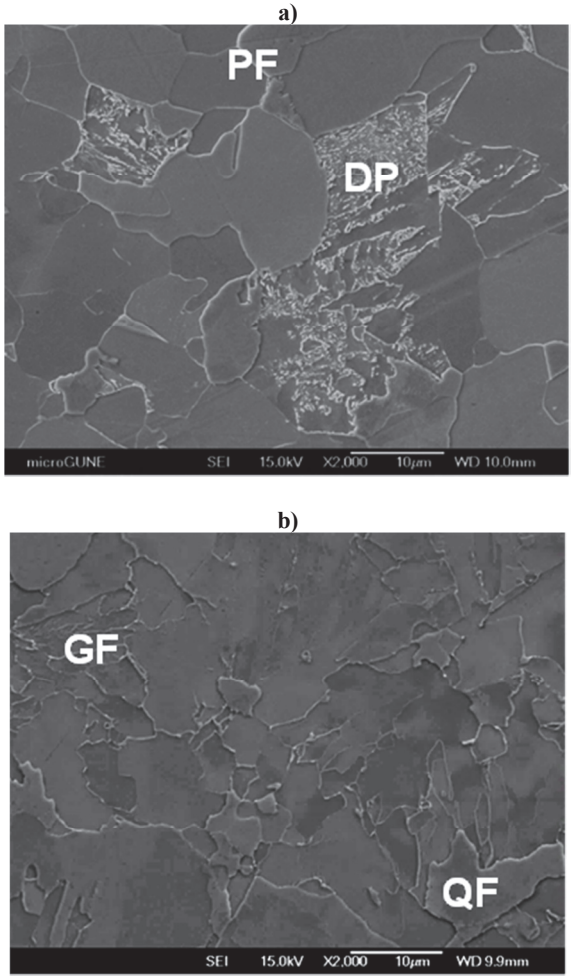

Fig. 11. *FEG-SEM micrographs of microstructures corresponding to Nb steel (S401) at the coiling temperatures 700ºC (a) and 600°C (b).*

6.3. Mechanical properties

The microstructures after coiling simulations were characterized and mechanical property evaluation (tensile and toughness) was performed, by means of hardness, tensile and Charpy tests. The improvement of mechanical properties is achieved via the control of microstructure, so a wide knowledge of the influence of process parameters on microstructure and therefore, on mechanical properties, is needed. The results relating the mechanical properties to the coiling temperature are summarised below.

Relations between yield stress and ultimate tensile strength and coiling temperature for the HSLA

steels were approximated by the second order polynomials:

$$\mathrm{Re} = a_0 + a_1 T_c + a_2 T_c^2 \qquad (56)$$

$$\mathrm{Rm} = b_0 + b_1 T_c + b_2 T_c^2 \qquad (57)$$

The coefficients in equations (56) and (57) for the HSLA steels are given in table 14.

Table 14. *The coefficients in equations describing mechanical properties of the HSLA steels.*

steel	a_0	a_1	a_2	b_0	b_1	b_2
S401 (Nb)	-951.41	4.7938	-0.004	-671.31	4.068	-0.0034
S403 (Nb+Mo)	-4214.2	16.442	-0.0136	-4380.5	17.247	-0.0143
S404 (Ti+Mo)	-3197.9	12.994	-0.0111	-3184.2	13.085	-0.0111

Finally, the model which predicts contribution of precipitates to the mechanical properties of the AHSS grades was tested. An increase of the yield stress calculated using equation (51) for cooling schedules characteristic for the hot strip mill is presented in figure 12. It is seen that contribution of precipitates is much larger for the steels containing titanium.

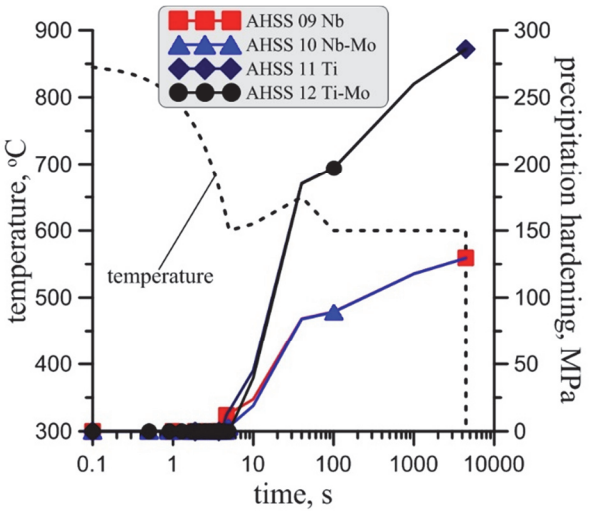

Fig. 12. *An increase of the yield stress calculated using equation (52) for cooling schedules characteristic for the hot strip mill.*

7. CONCLUSION

All the parameterized and validated models were saved in one database. Beyond this, the optimal coefficients obtained from the inverse analysis for all the models and all the steels were saved as well. In consequence the models needed at various stages of the manufacturing cycle are available for a large spectrum of steel grades. This aspect is especially important for engineers designing new process for new materials characterized by sophisticated behaviour. However, what is less visible but also crucial, is the usability of proposed database, which in this particular case is related to: database engine efficiency, easy access and scalability. The implementation of the database was performed by using state-of-the-art technologies in web application programming and document databases. This approach allowed to use high efficiency modern database engines aiming at fast and flexible collecting of data set. Furthermore, the implemented database was integrated with VirtRoll system, which made it easy to access through the RESTful architecture encapsulating all the functionalities offered by the database. Due to such solution this server-side application remains open and can be accessed by various end users. Finally, the scalability of proposed approach plays very important role by offering the opportunity to extend the created data sets with new material models equipped with new coefficients, simultaneously assuring to keep the efficiency at stable level independently of the final size of the database.

The integration of the database with the VirtRoll system guarantees fast and accurate simulations of the hot strip rolling, which in connection with optimization procedures and sensitivity analysis is a useful tool supporting technology design. Future extension of the database will be focused mainly on new data delivery being an effect of the inverse analysis procedure applied on results of various laboratory experiments.

ACKNOWLEDGEMENTS

Financial support of the MNiSzW, decision no. 2945/FBWiS/2013/2, in realization of the Research Fund for Coal and Steel (RFCS), project RFSR-CT-2013-00007, is acknowledged.

Resources of ACK Cyfronet AGH are acknowledged.

REFERENCES

Abad, R., Fernández, A.I., López, B., Rodriguez-Ibabe, J.M., 2001, Interaction between recrystallization and precipitation during multipass rolling in a low carbon niobium microalloyed steel, *ISIJ International*, 41, 1373-1382.

Andorfer, J., Auzinger, D., Hirsch, M., Hubmer, G., Pichler, R., 1998, VAI-Q strip – an online system for controlling the mechanical properties of hot rolled strip, *Proc. IFAC Workshop on Automation in Mining, Mineral and Metal Processing*, Cologne, 325-330.

Beynon, J.H., Sellars, C.M., 1992, Modelling microstructure and its effects during multipass hot rolling, *ISIJ International*, 32, 359-367.

Bhadeshia, H.K.D.H., 1980, The lower bainite transformation and the significance of carbide precipitation, *Acta Metallurgica*, 28, 1103-1114.

Davenport, S.B., Silk, N.J., Sparks, C.N., Sellars, C.M., 1999, Development of constitutive equations for the modelling of hot rolling, *Materials Science and Technology*, 16, 1-8.

Donnay, B., Herman, J.C., Leroy, V., Lotter, U., Grossterlinden, R., Pircher, H., 1996, Microstructure evolution of C-Mn steels in the hot deformation process: the STRIPCAM model, *Proc. Conf. Modelling of Metal Rolling Processes*, eds, Beynon, J.H., Ingham, P., Teichert, H., Waterson K., London, 23-35.

Gavrus, A., Massoni, E., Chenot, J.L., 1996, An inverse analysis using a finite element model for identification of rheological parameters, *Journal of Materials Processing Technology*, 60, 447-454.

Hensel, A., Spittel, T., 1979, *Kraft- und Arbeitsbedarf Bildsamer Formgebungs-verfahren*, VEB Deutscher Verlag fur Grundstoffindustrie, Leipzig.

Hodgson, P.D., Gibbs, R.K., 1992, A mathematical model to predict the mechanical properties of hot rolled C-Mn and microalloyed steels, *ISIJ International*, 32, 1329-1338.

Elwazri, A.M., Essadiqi, E., Yue, S., 2004, Kinetics of metadynamic recrystallization in microalloyed hypereutectoid steels, *ISIJ International*, 44, 744-752.

Ibrahim, M., Shulkosky, R., 2007, Simulation and development of Advanced High Strength Steels on a hot strip mill using a microstructure evolution model, *HSMM Application for AHSS*, 1 , 1-12.

Iza-Mendia, A., Gutiérrez, I., 2013, Generalization of the existing relations between microstructure and yield stress from ferrite–pearlite to high strength steels, *Materials Science Engineering A*, 561, 40-51.

Katsamas, A.I., Haidemenopoulos, G.N., 2008, A semi–empirical model for the evolution of retained austenite via bainitic transformation in multiphase TRIP steels, *Steel Research International*, 79, 875-884.

Kowalski, B., Sellars, C.M., Pietrzyk, M., 2000, Development of a computer code for the interpretation of results of hot plane strain compression tests, *ISIJ International*, 40, 1230-1236.

Król, D., Słota, R., Rauch, Ł., Kitowski, J., Pietrzyk, M., 2014, Harnessing heterogeneous computational infrastructures for studying metallurgical rolling processes, in: *eChallenges*, eds, Cunningham, P., Cunningham, M., International Information Management Corporation, Belfast, 1-9.

Kubin, L.P., Mortensen, A., 2003, Geometrically necessary dislocations and strain-gradient plasticity: a few critical issues, *Scripta Materialia*, 48, 119-125.

Kuziak, R., Pietrzyk, M., 2011,Physical and numerical simulation of the manufacturing chain for the DP steel strips, *Steel Research International*, special edition conf. ICTP, Aachen, 756-761.

Leblond, J.B., Devaux, J., 1984, A new kinetic model for anisothermal metallurgical transformations in steel including effect of austenite grain size, *Acta Metallurgica*, 32, 137-146.

Lenard, J.G., Pietrzyk, M., Cser, L., 1999, *Mathematical and physical simulation of the properties of hot rolled products*, Elsevier, Amsterdam.

Löffler, H., Döll, R., Poppe, T., Sörgel, G., Holtheuer, U., Zouhar, G., 2001, Control of mechanical properties by monitoring microstructure, *AISE Steel Technology*, 1, 44-47.

Lotter, U., Schmitz, H.-P., Zhang, L., 2004, Structure of the metallurgically oriented modelling system TK-StripCam for simulation of hot strip manufacture and application in research and production practice, *Journal de Physique IV France*, 120, 801-808.

McQueen, H.J., 1993, Controversies in the theory of dynamic recrystallization, *Materials Science Forum*, 113-115, 429-434.

Milenin, I., Pernach, M., Pietrzyk, M., 2015, Application of the control theory for modelling austenite-ferrite phase transformation in steels, *Computer Methods in Materials Science*, 15, 327-335.

Nanba, S., Kitamura, M., Shimada, M., Katsumata, M., Inoue, T., Imamura, H., Maeda, Y., Hattori, S., 1992, Prediction of microstructure distribution in the through-thickness direction during and after hot rolling in carbon steels, *ISIJ International*, 32, 377-386.

Novillo, E., Cotrina, E., Iza-Mendia, A., López, B. Gutiérrez, I., 2005, Factors limiting the achievable ferrite grain refinement in hot worked microalloyed steels, *Materials Science Forum*, 500-501, 355-362.

Pietrzyk, M., 1990, Finite element based model of structure development in the hot rolling process, *Steel Research*, 61, 603-607.

Pietrzyk, M., 2000, Finite element simulation of large plastic deformation, *Journal of Materials Processing Technology*, 106, 223-229.

Pietrzyk, M., 2002, Through-process modelling of microstructure evolution in hot forming of steels, *Journal of Materials Processing Technology*, 125-126, 53-62.

Pietrzyk, M., Kuziak, R., 2012, Modelling phase transformations in steel, in: *Microstructure evolution in metal forming processes*, eds, Lin, J., Balint, D., Pietrzyk, M., Woodhead Publishing, Oxford, 145-179.

Pietrzyk, M., Madej, Ł., Rauch, Ł., Szeliga, D., 2015, *Computational Materials Engineering: Achieving high accuracy and efficiency in metals processing simulations*, Elsevier, Amsterdam.

Pietrzyk, M., Kania, Z., Kuziak, R., Rauch, Ł., Kusiak, J., 2016, A simple model for prediction of retained austenite in steel rods after hot rolling and controlled cooling, *Proc. XXXV Verformungskundliches Kolloquium*, ed., Buchmayr, B., Zauchensee, 56-66.

Pietrzyk, M., Kuziak, R., Pidvysots'kyy, V., Kusiak, J., 2017, Applications of plane strain compression tests for identification of material models and for physical simulation of thermomechanical processing of bainitic steel, *Proc. XXXVI Verformungskundliches Kolloquium*, ed., Buchmayr, B., Zauchensee, 23-30.

Rauch, Ł., Bzowski, K., Kuziak, R., Kitowski, J., Pietrzyk, M., 2016, The off-line computer system for design of the hot rolling and laminar cooling technology for steel strips, *Journal of Machine Engineering*, 16, 27-43.

Sah, J.P., Sellars, C. M., Effect of deformation history on static recrystallization and restoration in ferritic stainless steels, 1979, *Proc. Conf. on Working and Forming Processes*, Metals Society, London, 62-66.

Sellars, C.M., McTegart, W.J., 1966, La relation entre la resistance et la structure dans deformation a chaud, *Mémoires et Etudes Scientifiques de la Revue de Metallurgie*, 63, 731-740.

Sellars, C.M., 1979, Physical metallurgy of hot working, in: *Hot Working and Forming Processes*, eds, Sellars, C.M., Davies, G.J., The Metals Soc., London, 3-15.

Smith, A., Miroux, A., Sietsma, J., van der Zwaag, S., 2006, A physical analysis of the stress relaxation kinetics of deformed austenite in C-Mn steel, *Steel Research International*, 77, 595-602.

Szeliga, D., Gawąd, J., Pietrzyk, M., 2006, Inverse analysis for identification of rheological and friction models in metal forming, *Computer Methods in Applied Mechanics and Engineering*, 195, 6778-6798.

Szeliga, D., Pietrzyk, M., 2007, Testing of the inverse software for identification of rheological models of materials subjected to plastic deformation, *Archives of Civil and Mechanical Engineering*, 7, 35-52.

Trowsdale, A.J., Randerson, K., Morris, P.F., Husain, Z., Crowther, D.N., 2001, MetModel: microstructural evolution model for hot rolling and prediction of final product properties, *Ironmaking and Steelmaking*, 28, 170-174.

Uranga, P., Fernandez, A.I., López, B., Rodriguez-Ibabe, J.M., 2004, Modeling of austenite grain size distribution in Nb microalloyed steels processed by thin slab casting and direct rolling (TSDR) route, ISIJ International, 44, 1416-1425.

Zahiri, S.H., Hodgson, P.D., 2004, The static, dynamic and metadynamic recrystallisation of a medium carbon steel, *Materials Science and Technology*, 20, 458-46.

Zurob, H.S., Hutchinson, C.R., Bréchet, Y., Purdy, G.R., 2004, Rationalization of the softening and recrystallization behaviour of microalloyed austenite using mechanism maps, *Materials Science and Engineering*, A 382, 64-81.

OPRACOWANIE BAZY DANYCH MATERIAŁOWYCH DLA KOMPUTEROWEGO SYSTEM VIRTROLL PRZEZNACZONEGO DO PROJEKTOWANIA OPTYMALNYCH TECHNOLOGII WALCOWANIA BLACH NA GORĄCO

Streszczenie

W artykule opisano bazę danych materiałowych, która została opracowana i zaimplementowana w komputerowym systemie VirtRoll przeznaczonym do projektowania optymalnych technologii walcowania blach na gorąco. W pierwszej części artykułu opisano strukturę i funkcjonalności bazy danych. W dalszej kolejności przedstawiono integrację bazy z systemem VirtRoll za pośrednictwem platformy Scalarm. Następne rozdziały artykułu są dedykowane generowaniu parametrów materiałowych, które zostały wprowadzone do bazy danych. Tymi parametrami są współczynniki w modelach materiałów obejmujących naprężenie uplastyczniające, rozwój mikrostruktury, przemiany fazowe i własności mechaniczne. Rozważono szereg modeli o różnym stopniu skomplikowania i różnych możliwościach obliczeniowych. Wszystkie modele należą do grupy modeli średniego pola (ang. mean field) i pozwalają na szybkie symulacje całego cyklu wytwarzania blach. Nowoczesne stale wielofazowe zostały wybrane jako przykłady obliczeniowe. Aby uzyskać dane do identyfikacji modeli wykonano badania doświadczalne obejmujące próby plastometryczne, relaksacji naprężeń i próby dylatometryczne. Identyfikację przeprowadzono z wykorzystaniem analizy odwrotnej. Dyskusja wyników została skupiona na walidacji modeli i na nowych aspektach modelowania.

Received: December 20, 2017
Received in a revised form: February 7, 2018
Accepted: April 16, 2018